Science of the Total Environment 659 (2019) 699–714

Contents lists available at ScienceDirect

Science of the Total Environment

journal homepage: www.elsevier.com/locate/scitotenv

Dual in-aquifer and near surface processes drive arsenic mobilization in Cambodian groundwaters

Laura A. Richards [a,*], Daniel Magnone [a,1], Jürgen Sültenfuß [b], Lee Chambers [c,2], Charlotte Bryant [d], Adrian J. Boyce [e], Bart E. van Dongen [a], Christopher J. Ballentine [a,3], Chansopheaktra Sovann [f], Sebastian Uhlemann [g,4], Oliver Kuras [g], Daren C. Gooddy [h], David A. Polya [a,*]

[a] School of Earth and Environmental Sciences and Williamson Research Centre for Molecular Environmental Science, The University of Manchester, Williamson Building, Oxford Road, Manchester M13 9PL, UK
[b] Institute of Environmental Physics, University of Bremen, Bremen 28359, Germany
[c] Lancaster Environment Centre, Lancaster University, Lancaster LA1 4YQ, UK
[d] NERC Radiocarbon Facility, Scottish Enterprise Technology Park, East Kilbride G75 0QF, UK
[e] Scottish Universities Environmental Research Centre, East Kilbride G75 0QF, UK
[f] Department of Environmental Science, Royal University of Phnom Penh, Phnom Penh, Cambodia
[g] British Geological Survey, Environmental Science Centre, Keyworth, Nottingham NG12 5GG, UK
[h] British Geological Survey, Maclean Building, Wallingford, Oxfordshire OX10 8BB, UK

HIGHLIGHTS

- Tracers used for monitoring groundwater evolution at a high spatial resolution.
- Groundwater arsenic associated with tracers of modern groundwater
- Surface-derived organic matter transported in aquifer to depths of >30 m.
- Groundwater arsenic accumulation rates are depth dependent.
- Dual in-aquifer and near surfaces processes drive arsenic mobilization.

GRAPHICAL ABSTRACT

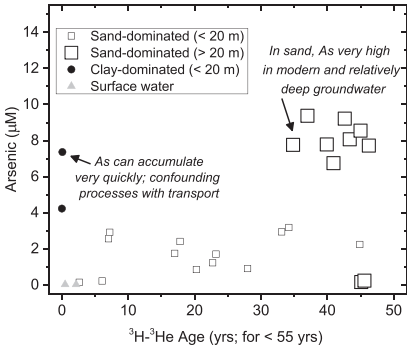

ARTICLE INFO

Article history:
Received 16 October 2018
Accepted 28 December 2018
Available online 29 December 2018

Editor: Filip M.G. Tack

Keywords:
Arsenic
Geochemical tracers

ABSTRACT

Millions of people globally, and particularly in South and Southeast Asia, face chronic exposure to arsenic from reducing groundwater in which arsenic release is widely attributed to the reductive dissolution of arsenic-bearing iron minerals, driven by metal reducing bacteria using bioavailable organic matter as an electron donor. However, the nature of the organic matter implicated in arsenic mobilization, and the location within the subsurface where these processes occur, remains debated. In a high resolution study of a largely pristine, shallow aquifer in Kandal Province, Cambodia, we have used a complementary suite of geochemical tracers (including ^{14}C, ^{3}H, ^{3}He, ^{4}He, Ne, $\delta^{18}O$, δD, CFCs and SF_6) to study the evolution in arsenic-prone shallow reducing groundwaters along dominant flow paths. The observation of widespread apparent ^{3}H-^{3}He ages of <55 years fundamentally challenges some previous models which concluded that groundwater residence times were on the order of hundreds

* Corresponding authors.
E-mail addresses: laura.richards@manchester.ac.uk (L.A. Richards), david.polya@manchester.ac.uk (D.A. Polya).
[1] Present address: School of Geography, University of Lincoln, Brayford Pool, Lincoln, Lincolnshire, LN6 7TS, UK.
[2] Present address: Department of Civil and Environmental Engineering, University of Strathclyde, Glasgow G1 1XJ, UK.
[3] Present address: Department of Earth Sciences, University of Oxford, South Parks Road, Oxford OX1 3AN, UK.
[4] Present address: Earth and Environmental Sciences Area, Lawrence Berkeley National Laboratory, Berkeley, CA, 94720, USA.

https://doi.org/10.1016/j.scitotenv.2018.12.437

Groundwater quality
Groundwater monitoring
Bioavailability

of years. Surface-derived organic matter is transported to depths of >30 m, and the relationships between age-related tracers and arsenic suggest that this surface-derived organic matter is likely to contribute to in-aquifer arsenic mobilization. A strong relationship between ^{3}H-^{3}He age and depth suggests the dominance of a vertical hydrological control with an overall vertical flow velocity of ~0.4 ± 0.1 m·yr^{-1} across the field area. A calculated overall groundwater arsenic accumulation rate of ~0.08 ± 0.03 μM·yr^{-1} is broadly comparable to previous estimates from other researchers for similar reducing aquifers in Bangladesh. Although apparent arsenic groundwater accumulation rates varied significantly with site (*e.g.* between sand *versus* clay dominated sequences), rates are generally highest near the surface, perhaps reflecting the proximity to the redox cline and/or depth-dependent characteristics of the OM pool, and confounded by localized processes such as continued in-aquifer mobilization, sorption/desorption, and methanogenesis.

1. Introduction

Millions of people in South and Southeast Asia face chronic exposure to groundwater containing dangerous concentrations of naturally-occurring arsenic (Smedley and Kinniburgh, 2002; Charlet and Polya, 2006; Ravenscroft et al., 2009; World Health Organization, 2011). Arsenic release in shallow aquifers typical to this region is widely attributed to the reductive dissolution of arsenic-bearing Fe(III) minerals (Islam et al., 2004). This process is driven by metal reducing bacteria and fuelled by electron donors provided by bioavailable organic matter (OM) (Charlet and Polya, 2006; Islam et al., 2004; Bhattacharya et al., 1997; van Geen et al., 2004; Postma et al., 2007; Rowland et al., 2009). Isotopic data, including ^{3}H, He, Ne, $\delta^{18}O$, δD, $\delta^{13}C$ and ^{14}C, have been used to probe the relative importance of various types of OM in driving such arsenic mobilization in a number of studies (Aggarwal et al., 2000; Harvey et al., 2002; van Geen et al., 2003; Lawson et al., 2008; Sengupta et al., 2008; van Dongen et al., 2008; McArthur et al., 2011; Neumann et al., 2011; Lawson et al., 2013; Lawson et al., 2016; Datta et al., 2011). The OM implicated is generally thought to originate, in some proportion, from (i) plant-derived OM internal to the sediment aquifers (Nickson et al., 1998; McArthur et al., 2001; McArthur et al., 2004); (ii) external, modern surface-derived OM, largely from ponds, rivers and rice paddies and transported through geomorphic features such as scroll bars, abandoned floodplains and meander channel deposits (Harvey et al., 2002; Lawson et al., 2013; Lawson et al., 2016; Polizzotto et al., 2008; Kocar et al., 2008; Papacostas et al., 2008; Neumann et al., 2010); and/or (iii) petroleum-derived hydrocarbons from thermally mature sediments at even greater depths (Rowland et al., 2009; van Dongen et al., 2008; Rowland et al., 2007; Al Lawati et al., 2012; Al Lawati et al., 2013; Magnone et al., 2017). The possible anthropogenic influence on arsenic mobilization due to large-scale groundwater abstraction remains unresolved (Harvey et al., 2002; van Geen et al., 2003; Sengupta et al., 2008; McArthur et al., 2011; Lawson et al., 2013; Neumann et al., 2010; Lawrence et al., 2000; Aggarwal et al., 2003; Harvey et al., 2003; Mailloux et al., 2013); for example increased abstraction could either increase arsenic hazard if bioavailable OM stimulates arsenic mobilization at a rate faster than recharge rates, or conversely, increased abstraction could decrease arsenic concentrations *via* dilution or "flushing" if surface water drawdown occurs at faster rates than arsenic mobilization (van Geen et al., 2008; Radloff et al., 2017). Debates surrounding the sub-surface location where OM undergoes initial depolymerisation and potential partial metabolic altercation and where initial arsenic mobilization takes place (*e.g.* near surface *versus* in-aquifer, noting the spatial and temporal continuum between surface and sub-surface), and the subsequent controls on arsenic mobility (Harvey et al., 2002; McArthur et al., 2011; Neumann et al., 2011; Lawson et al., 2013; Lawson et al., 2016; Datta et al., 2011; Schaefer et al., 2016; Stuckey et al., 2016), are intrinsically linked to the type (bioavailability) and amount of the OM implicated in arsenic release (Rowland et al., 2009; Harvey et al., 2002; van Dongen et al., 2008; Lawson et al., 2013; Lawson et al., 2016; Nickson et al., 1998; McArthur et al., 2004; Rowland et al., 2007; Al Lawati et al., 2012; Al Lawati et al., 2013; Gault et al., 2005; Neumann et al., 2009; Fendorf et al., 2010; Mladenov et al., 2010; Neumann et al., 2014). Determining the relative importance of these various inputs and clarifying these controls in dynamic alluvial systems are essential in determining how groundwater arsenic hazard may change in the future (Harvey et al., 2002; Lawson et al., 2016; Polya and Charlet, 2009).

Age tracers of modern (<50 years) groundwater (such as ^{3}H, CFCs and SF_6) are widely used in hydrological studies, including in the context of arsenic. Radioactive ^{3}H was released into the atmosphere in large quantities due to atmospheric thermonuclear testing between 1955 and 1963 (Solomon and Cook, 2000), with ^{3}H concentration in precipitation reaching a maximum of three orders of magnitude above natural concentrations in 1963. The ^{3}H decay product is the lighter and rare ^{3}He, and when used together, ^{3}H and ^{3}He can be used to date groundwater (Solomon and Cook, 2000; Tolstikhin and Kamenskiy, 1969; Weise and Moser, 1987; Schlosser et al., 1989; Szabo et al., 1996; Stute et al., 1997; Beyerle et al., 1999; Klump et al., 2006; Stute et al., 2007; Massmann et al., 2009; Sültenfuß et al., 2011). In the saturated zone, ^{3}He produced by ^{3}H decay accumulates in the groundwater and does not undergo any chemical transformation. Thus, derived ^{3}H-^{3}He ages are independent of the ^{3}H input concentration. ^{3}H-^{3}He dating in arsenic-affected aquifers in S/SE Asia has been carried out in a number of studies (Radloff et al., 2017; Klump et al., 2006; Stute et al., 2007; Postma et al., 2012; van Geen et al., 2013; McArthur et al., 2010), with young, arsenic-bearing groundwater having been observed up to ~20 m depth in Bangladesh (Stute et al., 2007) and up to ~40 m depth in Vietnam (van Geen et al., 2013) and in Cambodia (Lawson et al., 2016). The production of the greenhouse gases chlorofluorocarbons (CFCs), used for refrigeration and air-conditioning, began in the 1940s (CFC-12) and 1950s (CFC-11), and production of sulfur hexafluoride (SF_6), used as a thermal and electrical insulator, began in the 1960s (Plummer et al., 2006). Dissolved CFCs and SF_6 concentrations in groundwater have been widely used in hydrological studies as modern residence time indicators (Beyerle et al., 1999; Plummer et al., 2006; Cook and Solomon, 1995; Oster et al., 1996; Gooddy et al., 2006; Hinsby et al., 2007; Horneman et al., 2008; Darling et al., 2012; Jones et al., 2014), including in arsenic-impacted aquifers (Horneman et al., 2008; Lapworth et al., 2018). However, even though modern age tracers may indicate modern water at significant depths in arsenic-bearing aquifers (Aggarwal et al., 2000; Lawson et al., 2008; Lawson et al., 2013; Lawson et al., 2016; Klump et al., 2006; Dowling et al., 2003), this does not provide direct evidence of the involvement of surface or pond-derived OM in arsenic mobilization.

Groundwater arsenic concentrations are highly heterogeneous in shallow aquifers in Kandal Province, of the lower Mekong Basin, Cambodia (van Dongen et al., 2008; Lawson et al., 2013; Lawson et al., 2016; Polizzotto et al., 2008; Kocar et al., 2008; Polya and Charlet, 2009; Appelo and Postma, 1993; Polya et al., 2003; Polya et al., 2005; Tamura et al., 2007; Benner et al., 2008; Rowland et al., 2008; Gillispie et al., 2016; Richards et al., 2017a), an area which is relatively unaffected

by large-scale groundwater abstraction and thus representative of pre-development conditions. Simple proxies such as the mean grain size of the hosting sediment or proximity to rivers are not sufficient to explain the heterogeneity of groundwater arsenic, nor are seasonal changes in flow gradient and redox chemistry (Richards et al., 2017a). Rather, arsenic mobilization seems to be affected by complex surface-groundwater interactions, particularly in areas of high permeability and/or in close proximity to rivers or ponds, as well as by interactions within the aquifer (either near surface or deeper) which lead to a dual role for both surface and sedimentary OM in arsenic mobilization (van Dongen et al., 2008; Lawson et al., 2016). In order to better understand the nature of OM implicated in arsenic release (Rowland et al., 2009; Harvey et al., 2002; van Dongen et al., 2008; Lawson et al., 2013; Lawson et al., 2016; Nickson et al., 1998; McArthur et al., 2004; Rowland et al., 2007; Al Lawati et al., 2012; Al Lawati et al., 2013; Gault et al., 2005; Neumann et al., 2009; Fendorf et al., 2010; Mladenov et al., 2010; Neumann et al., 2014) and the location(s) within the subsurface where arsenic mobilization occurs (Harvey et al., 2002; McArthur et al., 2011; Neumann et al., 2011; Lawson et al., 2013; Lawson et al., 2016; Datta et al., 2011; Schaefer et al., 2016; Stuckey et al., 2016), a detailed understanding of the age and provenance of the groundwater is required at a resolution which captures local heterogeneity and the evolution of groundwater geochemistry along groundwater flowpaths. The aim of this study is thus to use a suite of geochemical tracers (including ^{14}C, ^{3}H, ^{3}He, ^{4}He, Ne, $\delta^{18}O$, δD, CFCs, SF_6 and OM bioavailability indicators) to probe the dominant geochemical controls on arsenic mobilization and accumulation in a high resolution study of a largely pristine shallow aquifer in Cambodia representative of pre-development conditions. Using a complementary suite of geochemical tracers, the specific objectives are to: (i) determine the age of groundwater and OM throughout the study area and its association with groundwater arsenic; (ii) examine the potential influence of preferential groundwater flowpaths and local heterogeneity on the overall geochemical conditions within the aquifer; and (iii) determine the dominant (hydro)geochemical controls on groundwater arsenic occurrence in such shallow, reducing aquifers typical of circum-Himalayan areas.

2. Methods and materials

2.1. Field site description and selection

The study region is in the Kien Svay district, northern Kandal Province, Cambodia, in the Lower Mekong Basin (Fig. 1), an area heavily affected by groundwater arsenic (Charlet and Polya, 2006; van Dongen et al., 2008; Lawson et al., 2013; Lawson et al., 2016; Polizzotto et al., 2008; Kocar et al., 2008; Polya and Charlet, 2009; Polya et al., 2005; Benner et al., 2008; Gillispie et al., 2016). Elevated levees along the Mekong and Bassac River banks retreat inland towards seasonally saturated wetlands, typical of the Lower Mekong Basin floodplains (Kocar et al., 2008; Magnone et al., 2017; Richards et al., 2017a). There is a seasonal control on the horizontal groundwater gradient, with groundwater flowing from the rivers inland during the monsoon season and in the reverse direction (inland towards the rivers) during the dry season (Benner et al., 2008; Richards et al., 2017a). The geomorphological framework of the study area is described elsewhere (Magnone et al., 2017). The field sites represent minimally-influenced, pre-development conditions given that large-scale groundwater abstraction in the area is very limited.

Two contrasting transects were initially selected using electrical resistivity tomography (ERT) (Uhlemann et al., 2017), which enabled identification of areas with contrasting resistivity and inferred hydraulic conductivity. The two transects are referred to as "T-Sand" (LR01–LR09) and "T-Clay" (LR10–LR14; Figs. 1 & 2) to reflect the largely sand-dominated and clay-dominated lithologies, respectively, of each area

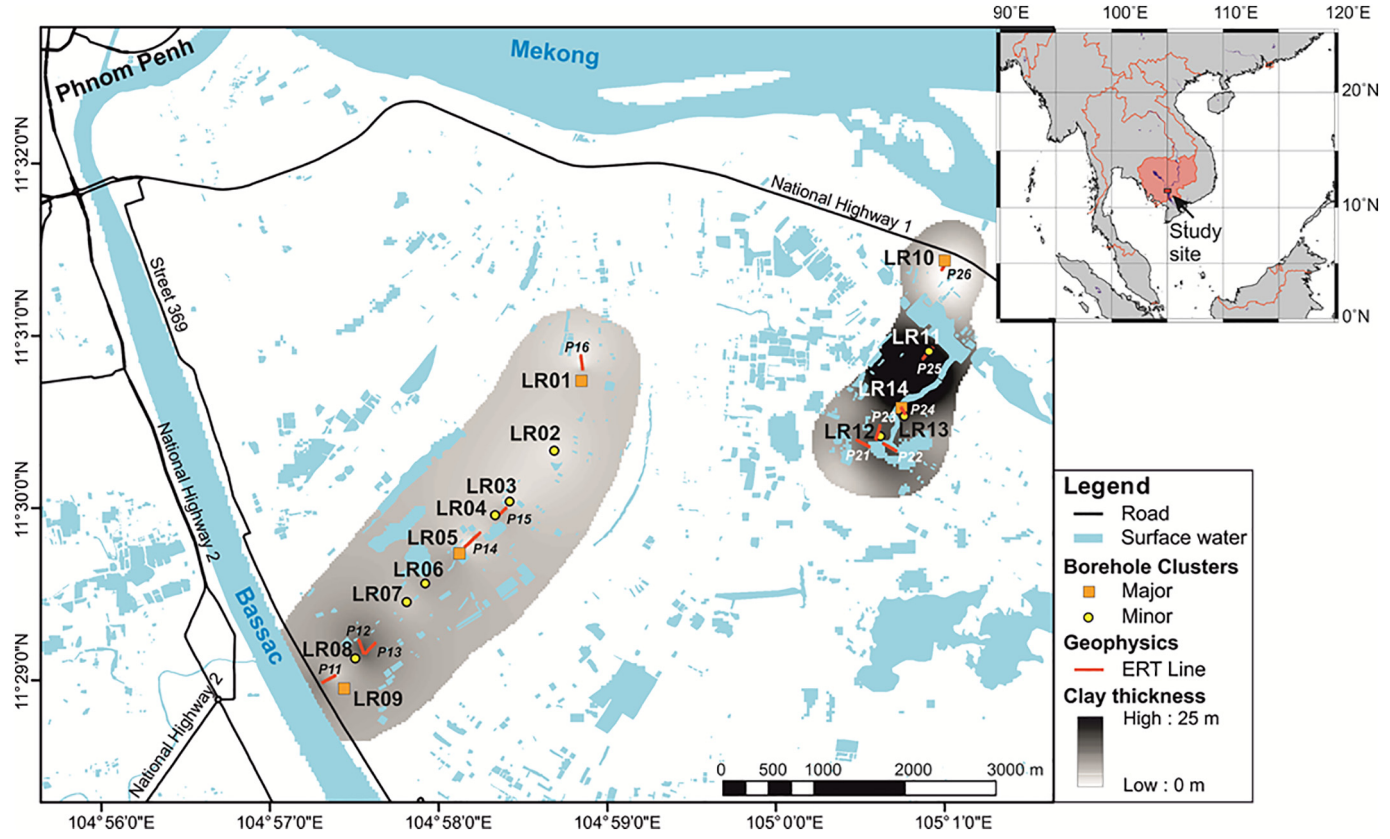

Fig. 1. Location of field area in northern Kandal Province, Cambodia, in the lower Mekong basin (Richards et al., 2017a; Richards et al., 2018). Field sites (LRxx), transects (T-Sand sites LR01–LR09; T-Clay sites LR10–LR14) along dominant groundwater flowpaths and electrical resistivity survey lines (ERT; Pxx) are shown (Uhlemann et al., 2017). The grey scale indicates clay thickness as informed by electrical resistivity tomography surveys (Uhlemann et al., 2017) and drillings logs.

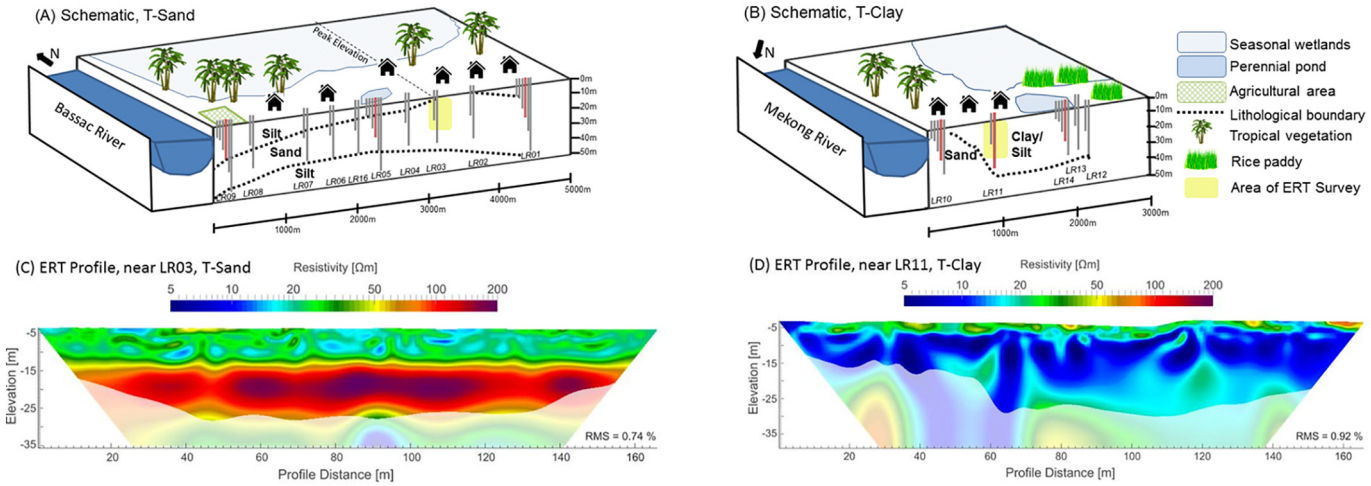

Fig. 2. Field site characterization (Richards et al., 2017a), including (A) and (B): Conceptual schematics of transects T-Sand and T-Clay, respectively, in northern Kandal Province, Cambodia illustrating the spatial construction of well nests for groundwater monitoring and sampling. Land influences include seasonal wetlands, ponds, agricultural areas and the Bassac and/or Mekong River. Red lines indicate locations of piezometric dataloggers; (C) and (D): Selected electrical resistivity tomography (ERT) profiles (Uhlemann et al., 2017) showing key differences in resistivity and inferred hydraulic conductivity at locations on T-Sand and T-Clay, respectively, near sites indicated by yellow boxes on A and B.

(Richards et al., 2017a). Specific sampling sites were oriented to be broadly parallel with major inferred groundwater paths, on the basis of topography, and were selected with landowner permission. Sampling sites were roughly located at equally spaced intervals across the 3–5 km transects. Prevalent land influences along each transect include seasonal wetlands, ponds and agricultural areas.

2.2. Well installation

Well clusters were installed during November 2013–February 2014 (Richards et al., 2015) using manual rotary drilling with a steel pipe (7.6 cm diameter) attached to a cutting auger (10.2 cm). Drilling fluid was continuously pumped through the pipe using a suction pump (Honda WB30XT, Cambodia). Wells were cased with PVC (6.97 cm inner diameter, Kandal Province, Cambodia) with 1 m of capped screening at the base. The outside of the casing was backfilled with weathered, locally available quartz-dominated alluvial gravel as the gravel pack, followed by backfilling with the original sediments and sealing with clay and concrete at the surface. The PVC casing protruded approximately 50 cm above the ground surface. High-permeability wells were developed by pumping compressed air (Yokohama GX-200, Japan) to the base of the casing; relatively low-permeability wells were developed using a submersible pump (Grundfos MP1, UK) or peristaltic pump (Geotech Easy Load II, UK). A lithium chloride tracer was used during drilling in order to quantify drilling-related contamination, which was shown to be minimal in developed wells (Richards et al., 2015). All wells were capped and locked when not in use, and closed/removed at the end of the study period.

At each of the 15 locations, 2–6 wells were installed (for a total of 49 wells), at the following depths: 6, 9, 15, 21, 30 and 45 m. Five sites (LR01, LR05, LR09, LR10, LR14) had clusters of 5 or 6 wells within several meters of each other spanning the full depth range (up to a maximum of 45 m for LR01, LR05 and LR09, and up to 30 m for LR10 and LR14), and all other sites had wells at 15 m and 30 m depths only. A schematic of the cluster layout is shown in Fig. 2. Wells were coded for identification as LRXX-YY where XX represents a specific site number and YY is the well depth in meters.

2.3. Sediment sampling

Wet sediment cores were collected at the time of drilling, typically every 3 m of depth, using a locally-designed stainless steel sampler, fitted internally with a replaceable extruded acrylic tube (25 mm outer diameter) and core-catcher. The sampler was inserted into the open centre of the steel pipe used for drilling and manually hammered for sample collection. Sediment cores were removed from the sampler immediately upon retrieval. Sediment cores subsampled for particle size analysis were stored in sealed polyethylene bags and frozen until subsequent analysis. Sediment cores for other analyses were stored anaerobically in furnaced aluminium foil bags, triple bagged in polyethylene and frozen (for inorganic/organic/^{14}C analysis) (Magnone et al., 2017).

2.4. Water sampling

Water sampling was conducted during two field seasons: (i) pre-monsoon in May–June 2014; and (ii) post-monsoon in November–December 2014 as previously described (Richards et al., 2017a). Groundwater (from a depth range of 6 to 45 m) and surface waters were sampled using a submersible pump (MP1, Grundfos) for wells >9 m in depth, and a peristaltic pump (Easy Load II Peristaltic Pump, Geotech Environmental Equipment, Inc.) for 6 and 9 m wells. Wells were flushed immediately prior to sample collection, until stabilization of E_h or after a maximum of pumping approximately 1.5 borehole volumes (Richards et al., 2015). Low yield wells were pumped dry with re-infiltrated water and sampled within the following one to three days. Surface water was collected from approximately 0.5 m below the water/air interface with the same sample treatment as groundwater.

Subsamples of ground- and/or surface water were collected, filtered (0.45 μm cellulose/polypropylene syringe filters, Minisart RC, UKs), and acidified to pH < 2 (trace grade nitric acid, BDH Aristar, UK) for analysis of cations and dissolved organic carbon (DOC) (Richards et al., 2017a). Filtered subsamples were left unacidified for analysis of anions and fluorescence measurements. Subsamples collected for cation, anion and DOC analysis were stored in 100 mL glass Schott bottles (or 30 mL for fluorescence measurements), which were acid-washed and furnaced before use to remove trace contamination. Subsamples for field-based arsenic speciation (Watts et al., 2010) were collected using resin-based ion-exchange cartridges (Bond Elut Jr. SCX 12162040B and Bond Elut Jr. SAX, 12162044B, both Agilent UK).

Water subsamples for ^{3}H analysis were collected in duplicate in 1 L argon filled amber glass bottles and stored with an approximately 4 cm head of argon gas. Water subsamples for noble gas (He and Ne)

analysis were collected in duplicate in flushed soft copper tubes, manually clamped using stainless steel clamps mounted on aluminium racks (Richards et al., 2017b). A regulator clip was attached to a short transparent hose connected to the outlet of the copper tube and narrowed to increase pressure to suppress potential degassing. Samples tubes were clamped on the outlet end prior to the inlet. Groundwater subsamples for stable isotopes (δD and δ^{18}O) were not filtered nor chemically preserved and were collected in 60 mL acid-washed and furnaced amber glass Schott bottles with polyseal caps (Richards et al., 2018). Water subsamples for ^{14}C-TOC were collected in 2.5 L amber glass bottles, unfiltered, and samples (~500 mL) for ^{14}C-TIC were collected using 1 L capacity foil bags (FlexFoil PLUS), which had been adapted for water sampling, pre-flushed with nitrogen and sample rinsed (Bryant et al., 2013). Subsamples for CFCs and SF_6 were collected by the USGS single bottle method using a 'diffusion barrier' to avoid re-equilibration with the atmosphere (Plummer et al., 2006; Darling et al., 2012). All samples were placed in field coolers within 60 min of collection and refrigerated (approximately 4 °C) within several hours, with the exception of ^{14}C-TIC samples which were frozen and ^{3}H, CFC, SF_6 and noble gas subsamples which were not refrigerated. Samples for methane (CH_4) analysis were collected into double-valve steel cylinders of known capacity.

2.5. Sediment analytical measurements

Sediment colour, description and visual grain size categorisation was recorded in the field at the time of drilling. Particle size analysis was completed at the British Geological Survey (Keyworth, UK) using laser diffraction (LS 13 320 Laser Diffraction Particle Size Analyzer, Beckman Coulter, UK) with statistical analysis *via* Gradistat_v8 software (Richards et al., 2017a). Contour plots of grain size were produced using OriginPro 2015 and supplemented with drilling logs.

Sedimentary ^{14}C (as total carbon following exposure to concentrated hydrochloric acid fumes) was prepared and analysed at the NERC Radiocarbon Facility (East Kilbride, UK) using methods previously described (Magnone et al., 2017). In brief, pre-treatment consisted of placing samples into pre-cleaned beakers, covered by pre-cleaned glass fibre filter papers and placed into a desiccator (without desiccant) together with concentrated hydrochloric acid to hydrolyse any carbonate in the sample by fumigation. The desiccator was evacuated, isolated and heated for the internal temperature of the desiccator, acid and samples to reach 63 $\pm$ 2 °C. The samples were removed from the desiccator after 24 h, stirred to ensure full exposure to acid fumes and fumigated for a further 24 h. Total carbon in a known weight of pre-treated sample was recovered as CO_2 following combustion in sealed quartz tubes (Boutton et al., 1983), in the presence of copper oxide and silver, and cryogenically isolated and converted to graphite by Fe/Zn reduction (Slota et al., 1987).

2.6. Aqueous analytical measurements

2.6.1. Inorganic and organic analysis

Measurements on aqueous samples were conducted both in field and laboratory settings (Richards et al., 2017a). Field measurements included pH, oxidation-reduction potential (*Eh*), dissolved oxygen and conductivity/temperature, which were collected *in-situ* using a multimeter (Professional Plus Series Portable Multimeter, YSI), equipped with probes/sensors (605101, 605102, 605203 and 605301, respectively, YSI, UK) and a flow-through cell (603059, YSI, UK). *In-situ* analysis of selected chemical parameters was conducted immediately following sample collection using a field spectrophotometer (Spectroquant Nova 60A, Merck, Germany) and appropriate test kits (Richards et al., 2017a; Richards et al., 2015). Cations were analysed using inductively coupled plasma atomic emission spectrometer (ICP-AES, Perkin-Elmer Optima 5300 dual view) and/or inductively coupled plasma mass spectrometry (ICP-MS, Agilent 7500cx; including for arsenic), both located within the Manchester Analytical Geochemistry Unit (MAGU) at The University of Manchester (Richards et al., 2017a). Anions were analysed using ion chromatography (IC; Dionex ICS5000 Dual Channel Ion Chromatograph) at MAGU.

Excitation-emission matrix fluorescence analysis was undertaken at BGS Wallingford using a fluorescence spectrometer (Varian™ Cary Eclipse) and interpreted using parallel factor analysis (Stedmon et al., 2003; Stedmon and Bro, 2008) to determine a fluorescence-based OM bioavailability proxy (β:α), relating to the relative amounts of labile DOM (β, often microbially produced or autochthonous/*in-situ*) to recalcitrant terrestrial carbon (α, allochthonous) (Parlanti et al., 2000; Wilson and Xenopoulos, 2009; Kulkarni et al., 2017), and which was calculated using R software (Lapworth and Kinniburgh, 2009). Methane was analysed at BGS Wallingford using a headspace technique and gas chromatography as previously reported (Gooddy and Darling, 2005; Darling and Gooddy, 2006; Bell et al., 2017).

2.6.2. Analysis of ^{3}H, he isotopes and ne

Analysis of ^{3}H, He isotopes (^{3}He and ^{4}He) and Ne were conducted at the Helis Noble Gas Laboratory (Institute of Environmental Physics, University of Bremen, Germany) using methods previously described (Sültenfuß et al., 2009a). All gases were extracted from the water for He isotope and Ne analysis, with He and Ne separated cryogenically from other gases, at 25 and 14 K, respectively. ^{4}He and Ne were measured with a quadrupole mass spectrometer (Balzers QMG112A) and He isotopes with a high-resolution sector-field mass spectrometer (MAP 215–50). The system was calibrated with atmospheric air and controlled for stable conditions for the He and Ne concentrations and the ^{3}He/^{4}He ratio. The analytical precision is typically <1% for the He and Ne concentrations and <0.5% for the ^{3}He/^{4}He ratio.

^{3}H in water samples was analysed using the ^{3}He-ingrowth method (Clarke et al., 1976), where water samples were degassed and stored for the accumulation of the ^{3}H decay product ($^{3}He_{sample}$). $^{3}He_{sample}$ was measured after an in-growth period of approximately six months using the mass spectrometer (MAP 215-50). The detection limit of ^{3}H analysis was 0.02 TU. Separation of noble gas components and the associated calculation of apparent ^{3}H-^{3}He model ages was conducted as previously described, including using measured Ne and calculated Ne equilibrium concentrations to estimate excess ^{3}He, and measured ^{4}He to estimate radiogenic ^{3}He (Sültenfuß et al., 2011) (see Section 2.7 for calculation details).

2.6.3. CFCs and SF_6

CFCs and SF_6 were measured at the British Geological Survey (Wallingford, UK) by gas chromatography with an electron capture detector, following 'purge and trap' cryogenic pre-concentration (Busenberg and Plummer, 2000), with a detection limit of 0.01 pmol·L^{-1} and 0.1 fmol·L^{-1}, respectively (Gooddy et al., 2006). The CFCs and SF_6 are calibrated to bulk air standards from the Advanced Global Atmospheric Gases Experiment (AGAGE) atmospheric monitoring network. Ne data was used to correct CFCs and SF_6 for excess air/degassing. SF_6 "piston flow" ages (with no mixing) were determined by comparison of Ne-corrected SF_6 measurements with the Northern Hemisphere atmospheric air equilibrium concentration (United States Geological Survey (USGS), 2017) of SF_6 at 27.7 °C, approximately the average annual temperature in Cambodia (Thoeun, 2015). CFCs were excluded from age calculations due to partial degradation of CFCs occurring in some cases. Ground gas samples from selected locations within the field area were obtained to validate the applicability of global CFC-11, CFC-12 and SF_6 input functions for groundwater dating (Darling and Gooddy, 2007).

2.6.4. ^{14}C-TOC and ^{14}C-TIC

Groundwater ^{14}C-TOC and ^{14}C-TIC were prepared and analysed at the NERC Radiocarbon Facility (East Kilbride, UK). Samples for the analysis of ^{14}C-TOC were pre-treated by freeze-drying measured sample volumes and transferred into a desiccator (without desiccant) in

beakers covered by glass fibre filter papers. Carbonate in the sample was hydrolysed with concentrated hydrochloric acid. The desiccator was evacuated with a vacuum pump and the internal temperature of the desiccator, acid and samples was controlled to be 63 ± 2 °C. The total carbon was recovered as CO_2 following combustion in a silver capsule using an elemental analyzer (Costech Instruments ECS 4010, Italy). The gas was cryogenically isolated and converted to graphite by Fe/Zn reduction. Groundwater samples for ^{14}C-TIC were defrosted approximately 8 h before hydrolysis with 85% ortho phosphoric acid and purging with He to recover CO_2 from total inorganic carbon. The recovered gas was cryogenically isolated and converted to graphite by Fe/Zn reduction. ^{14}C analysis of graphite was conducted at the Scottish Universities Environmental Research Centre (SUERC, East Kilbride, Scotland, UK) on either a 5 MV tandem accelerator mass spectrometer or 250 kV single stage accelerator mass spectrometer (both National Electrostatics Corporation, USA) (Xu et al., 2004; Freeman et al., 2010). Consistent with international practice, ^{14}C results are reported as measured % modern ^{14}C (pmC) and well as conventional radiocarbon years BP (relative to AD 1950) for ^{14}C-TOC (Magnone et al., in review). Results have been corrected to a $\delta^{13}C_{VPDB}$ of −25‰ using δ^{13}C as measured on a sub-sample of CO_2 from the original, pre-treated sample material on a dual inlet stable isotope mass spectrometer with multiple ion beam collection (Thermo Fisher Delta V, Germany). Groundwater ^{14}C analysis from two NRCF Allocations (1835.0714 and 1906.0415) were undertaken; however due to unresolved concerns about the impact of prolonged storage prior to sample preparation on ^{14}C and ^{13}C isotopic compositions for the 1906.0415 allocation (dominantly post-monsoon samples), only results from the 1835.0714 allocation (pre-monsoon samples) are reported here. Stable isotope analysis (δD and δ^{18}O) (Richards et al., 2018) was conducted at the Isotope Community Support Facility (ICSF) at SUERC using standard techniques (Donnelly et al., 2001).

2.7. Derivation of ^{3}H-^{3}He model ages

^{3}H concentrations in water are expressed in tritium units (TU; 1 TU = 10^{-18} ^{3}H/^{1}H). Tritiogenic ^{3}He (^{3}He$_{tri}$) is produced by ^{3}H decay (1 TU = $2.49 \cdot 10^{-12}$ ^{3}He$_{tri}$ cm^{3}STP·kg^{-1} water; STP = standard temperature and pressure). An apparent ^{3}H-^{3}He age, τ, the mean residence time between last atmospheric contact and the measurement date, is given in Eq. (1) by

$$\tau = \frac{1}{\lambda} \cdot \ln 1 + \frac{^3He_{tri}}{^3H} \quad (1)$$

where λ is the decay constant ($\lambda = \ln(2)/t_{1/2}$; $t_{1/2}$ (^{3}H half-life) = 12.32 years (Lucas and Unterweger, 2000)). ^{3}He$_{tri}$ must be separated from other sources of ^{3}He (Sültenfuß et al., 2011), namely:

I. Equilibrium ^{3}He (^{3}He$_{equil}$): concentration at atmospheric equilibrium, dependent on temperature, salinity and atmospheric pressure during infiltration; calculated with Weiss' solubility function (Weiss, 1971), with isotopic fractionation ($\alpha = 0.983$ (Benson and Krause, 1980)) and the atmospheric ratio (^{3}He/^{4}He$_{atmos}$ = $1.384 \cdot 10^{-6}$ (Clarke et al., 1976)), per Eq. (2):

$$^3He_{equil} = {}^4He_{equil} \cdot \left(\frac{^3He}{^4He}\right)_{atmos} \cdot \alpha \quad (2)$$

II. Excess ^{3}He (^{3}He$_{excess}$): additional/excess atmospheric air dissolved in the water from the (partial) dissolution of air bubbles trapped in the quasi saturated soil zone (Aeschbach-Hertig et al., 2008) and may be linked in part to the seasonally fluctuating water table. This component is calculated from Ne, which has no in-aquifer sources, *via* the deviation of Ne (Δ Ne, %) in the sample (Ne$_{sample}$) from the calculated air-saturated equilibrium (Ne$_{equil}$), with the atmospheric ratio (^{4}He/Ne$_{atmos}$ = $2.88 \cdot 10^{-1}$ (Schlosser et al., 1989)), per Eqs. (3) and (4):

$$\Delta Ne = \left(\frac{Ne_{sample}}{Ne_{equil}} - 1\right) \cdot 100 \quad (3)$$

$$^3He_{excess} = (Ne_{sample} - Ne_{equil}) \cdot \left(\frac{^4He}{Ne}\right)_{atmos} \cdot \left(\frac{^3He}{^4He}\right)_{atmos}, \quad (4)$$

III. Radiogenic ^{3}He (^{3}He$_{rad}$): produced naturally from sediments and subsequently released into water; aqueous concentrations of ^{3}He$_{rad}$ are small and derived from radiogenic ^{4}He (^{4}He$_{rad}$), with ^{3}He$_{rad}$/^{4}He$_{rad}$ ratios on the order of 10^{-8} (Andrews, 1985). ^{4}He$_{rad}$ is produced by α-decay of nuclides from the decay series of uranium and thorium and can be used as a qualitative age indicator and was calculated as in Eq. (5):

$$^4He_{rad} = {}^4He_{sample} - {}^4He_{equil} - {}^4He_{excess} \quad (5)$$

Therefore, ^{3}He$_{tri}$ as used to calculate τ was calculated by Eq. (6):

$$^3He_{tri} = {}^3He_{sample} - {}^3He_{equil} - {}^3He_{excess} - {}^3He_{rad} \quad (6)$$

where ^{3}He$_{sample}$, ^{4}He$_{sample}$ and Ne$_{sample}$ are measured, and ^{3}He$_{equil}$, Ne$_{equil}$, ^{3}He$_{excess}$, ^{4}He$_{equil}$, ^{4}He$_{excess}$ and ^{4}He$_{rad}$ are calculated. The assumptions included: (i) infiltration conditions of 30 °C temperature and 50 m altitude; (ii) complete dissolution of air bubbles which maintain atmospheric noble gas ratios; (iii) equally proportional gas loss during degassing; (iv) ^{3}He$_{rad}$/^{4}He$_{rad}$ ≈ $2 \cdot 10^{-8}$ (Mamyrin and Tolstikhin, 1984); and (v) negligible mantle ^{3}He contribution (^{3}He$_{mantle}$) to terrigenic ^{3}He (^{3}He$_{terr}$) (*e.g.* ^{3}He$_{terr}$ = ^{3}He$_{mantle}$ + ^{3}He$_{rad}$, where ^{3}He$_{mantle}$/^{3}He$_{rad}$ < $1 \cdot 10^{-5}$; thus ^{3}He$_{terr}$ ≈ ^{3}He$_{rad}$).

The uncertainties associated with ^{3}He$_{tri}$ and thus apparent ^{3}H-^{3}He age calculations include solubility data (*e.g.* equilibrium concentration, temperature, altitude and salinity), He components (*e.g.* atmospheric ^{3}He/^{4}He, ^{3}He/^{4}He of other sources, terrigenic ^{3}He/^{4}He), excess air (*e.g.* atmospheric volume ratios, excess air models and associated parameters) and analytical errors (Sültenfuß et al., 2009b). Uncertainties in ^{3}H$_{tri}$ and ^{3}H-^{3}He ages are approximately ±0.5 TU and ± 2 years, respectively (Sültenfuß et al., 2009b), with ^{3}H-^{3}He duplicates typically in agreement to within ±1 year. All ^{3}H-^{3}He ages are reported on a 2014 sampling basis.

2.8. Quality assurance and quality control

The quality assurance/quality control (QA/QC) measures undertaken during sampling and inorganic analysis are described in detail elsewhere (Richards et al., 2017a; Polya and Watts, 2017; Polya et al., 2017). Quality control for ^{14}C, including determining the overall analytical precision, involved processing international standards and background materials through all the pre-treatment and preparation methods used for the samples, size-matched to cover the range of sample sizes. International standards were used during AMS analysis, including backgrounds and NIST Oxalic Acid II. For small samples (<500 μg C), further size matched standards and backgrounds were used to calculate appropriate sample size related ^{14}C results. The Costech mass spectrometer was calibrated with international reference materials to a precision of ±0.1 $\delta^{13}C_{VPDB}$‰. All statistical analysis was conducted using Origin 2016; regression statistics are reported as *"t(degrees of freedom) = t value; p = p value"* at 95% confidence.

3. Results and discussion

3.1. Dominant groundwater geochemistry and arsenic distribution

In a largely unperturbed Cambodian aquifer representative of pre-groundwater development conditions in the lower Mekong Basin (Figs. 1 and 2), natural concentrations of dissolved arsenic range from ~0.02 to >14 μM (~2–1100 $\mu g \cdot L^{-1}$), with >90% of samples (n = 72) exceeding the World Health Organization provisional guideline value of 0.13 μM (10 $\mu g \cdot L^{-1}$) (World Health Organization, 2011; Richards et al., 2017a). Concentrations of arsenic, occurring mostly as inorganic As^{III}species, typically increase with depth and vary substantially over both lateral and vertical spatial profiles; detailed profiles of the variation of arsenic (including speciation), iron and redox-sensitive parameters (*e.g.* dissolved oxygen, sulfate, nitrate, nitrite ammonium, *etc.*) are published elsewhere (Richards et al., 2017a). Groundwater chemistry is dominated by calcium, magnesium and bicarbonate, typical of most arsenic-bearing groundwaters in S/SE Asia (Smedley and Kinniburgh, 2002; Lawson et al., 2013; Polizzotto et al., 2008; Richards et al., 2017a). The variation of iron, sulfate and dissolved oxygen is consistent with arsenic mobilization *via* reductive dissolution of iron (hydr)oxides (Islam et al., 2004; Lawson et al., 2013; Lawson et al., 2016; Kocar et al., 2008; Richards et al., 2017a). Seasonal variations in groundwater geochemistry (especially sulfate and dissolved oxygen concentrations), particularly at shallow depths near sites where surficial clays are thin or absent (*e.g.* LR01 and LR02), or near rivers (*e.g.* LR10) and/or ponds (*e.g.* LR05 and LR14), are indicative of "fast track" zones where rapid monsoonal surface water incursion may occur (Richards et al., 2017a; Richards et al., 2018; Uhlemann et al., 2017). Stable isotope (δD and $\delta^{18}O$) data show that groundwater with high arsenic can be recharged both by evaporated surface water as well as local precipitation (Richards et al., 2018).

3.2. Tritium (^3H) and tritium-helium (^3H-^3He) model ages

Tritium (^3H) signatures and tritium-helium (^3H-^3He) model ages provide direct, unequivocal evidence that modern (<55 years) groundwater is present in these aquifers even up to depths of 45 m (Fig. 3A) (Richards et al., 2017b). This evidence fundamentally challenges previous models which simulated groundwater residence times on the order of hundreds of years in this same area in Cambodia (Polizzotto et al., 2008; Benner et al., 2008), but is consistent with young groundwater having been observed at relatively shallow depths (*e.g.* on the order of 10s of meters) elsewhere in S/SE Asia, including Bangladesh (Stute et al., 2007) and Vietnam (van Geen et al., 2013). A strong relationship between ^3H-^3He age and depth ($t = 5.1$; $p < 0.01$) suggests the dominance of a vertical hydrological control (Figs. 3A and 4). This allows an estimation of an overall vertical flow velocity of ~0.4 ± 0.1 $m \cdot yr^{-1}$ across the whole study area, with apparent horizontal flow velocities ~40 to 170 $m \cdot yr^{-1}$. Site-specific age-depth profiles (Fig. 3B) allow the estimation of localized vertical flow velocities (ranging from ~0.5–1.6 $m \cdot yr^{-1}$ at a particular location) and identification of relatively high permeability zones, particularly near sandy windows in near surface clayey layers and/or ponds (*e.g.* near sites LR01, LR05 and LR10), consistent with the inferred distribution pf hydraulic conductivity as indicated from geophysical characterization (Uhlemann et al., 2017) and where seasonal changes in sulfate and dissolved oxygen in shallow samples were observed (Richards et al., 2017a). This site-specific heterogeneity is consistent with heterogeneity captured in surface expressions of Pleistocene sands in the local study area in the lower Mekong (Gillispie et al., 2016) as well as projections for other prograding deltas such as the Ganges-Brahmaputra (McArthur et al., 2008), and highlights the unsuitability of simple layered homogeneous models (Polizzotto et al., 2008; Benner et al., 2008). The consistency of 'initial tritium' (the sum of ^3H and tritiogenic ^3He ($^3He_{tri}$)) with the independent input function for Bangkok precipitation (IAEA/WMO, 2015) suggests that no old ^3H-free groundwater is admixed with young water in the majority of the groundwater (Fig. 3C). The apparent limited mixing is consistent with the relatively low hydraulic gradient and limited groundwater abstraction in the area, although monsoon-driven reversal in groundwater flow-direction (Kocar et al., 2008; Benner et al., 2008; Richards et al., 2017a) will likely still impact localized flow regimes.

Particularly along T-Clay (Figs. 3A & 4B), the inferred rate of recharge indicates preferential flow regimes and suggests a layered, multi-porosity domain, with very young age and rapid recharge shown in shallower samples (*e.g.* LR10-15) and much older age in deeper samples (*e.g.* LR10-30). This is perhaps not surprising given the fractured nature of clays, however the important implication is that the overall aquifer (bio)geochemistry in such areas will likely be controlled by flow-controlled exchange between relatively small volumes of groundwater originating from a high conductivity zone with groundwater from a low conductivity zone.

3.3. CFC and SF_6 groundwater signatures

Modern indicators CFC-11, CFC-12 and SF_6 (Table 1) were detected in most samples with several exceptions, noting that analytical interferences prohibited measurement of CFC-12 in some samples. The detection of CFCs and SF_6 in most samples confirms the modern nature of groundwater as indicated by ^3H and apparent ^3H-^3He ages. All concentrations of CFC-11, CFC-12 and SF_6, with Ne-based corrections for excess air/degassing, are within feasible ranges for air equilibrated water under

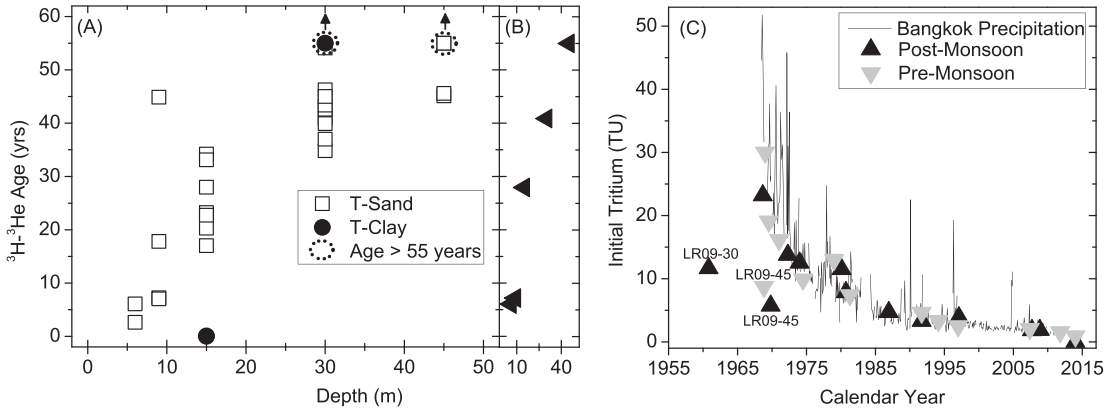

Fig. 3. (A) Apparent groundwater ^3H-^3He age *versus* depth along sand-dominated "T-Sand" and clay-dominated "T-Clay" transects (Figs. 1 & 2) (Richards et al., 2017a) shows 80% of groundwater is modern (<55 years in ^3H-^3He age) with overall vertical flow velocity of ~0.4 ± 0.1 $m \cdot yr^{-1}$ (*t-value = 5.1; p-value ≪ 0.001;* ages <55 years excluding samples below input); (B) ^3H-^3He age-depth single site profile at sand-dominated LR01 (data on B is also included in A); (C) 'Initial tritium' (^3H plus $^3He_{tri}$) for pre- (grey) and post-monsoon (black) groundwater with the Bangkok input function (IAEA/WMO, 2015). ^3H and ^3H-^3He ages are broadly consistent with SF_6 data (Fig. 5).

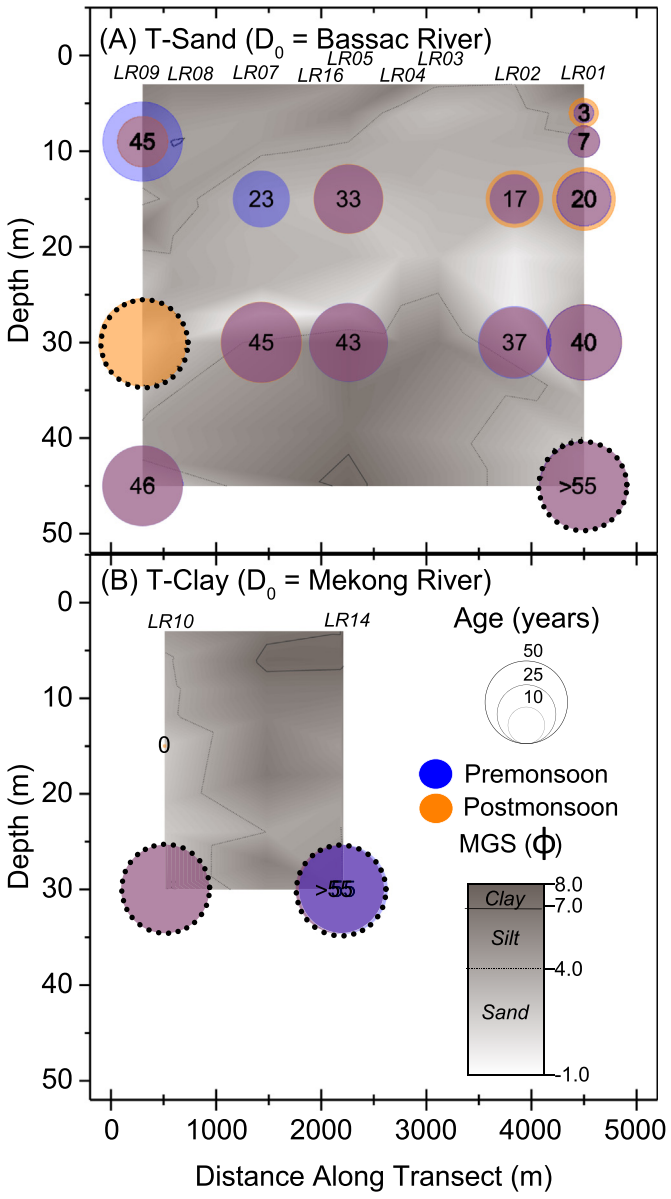

Fig. 4. Spatial distribution of apparent ^{3}H-^{3}He age (in years, 2014 basis) in the (A) T-Sand and (B) T-Clay transects. Distance refers to that from the Bassac and Mekong Rivers, respectively). Labelled ages are from pre-monsoon samples (*e.g.* blue coded) with changes between seasons noted by changes in bubble size. Dashed lines indicate samples with apparent ages >55 years. High permeability zones of rapid recharge are identified particularly around LR05, LR01 and LR02 on T-Sand and LR10 on T-Clay. The underlying greyscale contour represents sedimentary mean grain size with approximate distinctions between clay/silt/sandy domains.

recharge conditions, suggesting that there is no in-aquifer contamination of CFCs (Darling et al., 2012; Morris et al., 2006a; Morris et al., 2006b) or SF_6 (Fulda and Kinzelbach, 2000; Santella et al., 2008). There are several indications that degradation of both CFC-11 and CFC-12 has occurred (with preferential degradation of CFC-11), including that generally (i) CFC-11 is lower than would be expected based on CFC-12 concentrations and (ii) CFC-12 is lower than would be expected based on SF_6 concentrations. Such degradation of CFCs is commonly observed and widely attributed to microbial breakdown, particularly in anoxic conditions, which typically affects CFC-11 preferentially (Oster et al., 1996; Hinsby et al., 2007; Horneman et al., 2008; Khalil and Rasmussen, 1989). The apparent CFC degradation highlights the importance of co-occurring processes such as microbially-driven OM breakdown (Fendorf et al., 2010). The apparent degradation of CFCs limits its quantitative application in simple steady-state lumped parameter models, although the elevated CFC-11 and CFC-12 concentrations still qualitatively indicate the presence of modern groundwater inputs.

Table 1
Measured Ne, CFC-11, CFC-12 (pmol·L^{-1}) and SF_6 (fmol·L^{-1}) in post-monsoon groundwater samples with Ne-based corrections (corr) for degassing/excess air. The SF_6 age represents a "piston flow" age with no mixing as estimated by comparison of measured values with atmospheric equilibrium concentrations. The theoretical concentrations of CFC-11, CFC-12 and SF_6 in air equilibrated water at 27.7 °C, approximately the mean annual temperature in Cambodia (Thoeun, 2015), are 2.08 pmol·L^{-1}, 1.34 pmol·L^{-1} and 1.70 fmol·L^{-1}, respectively.

Sample ID	Ne (cm^3 STP·g^{-1})	CFC-11$_{corr}$ (pmol·L^{-1})	CFC-12$_{corr}$ (pmol·L^{-1})	$SF_{6,cor}$ (fmol·L^{-1})	SF_6 Age (yrs)
LR01-15-POST	1.24E−07	0.14	0.55	0.74	22
LR01-30-POST	2.08E−07	<0.01	0.17	0.42	29
LR01-45-POST	2.50E−07	<0.01	0.11	0.12	40
LR01-6-POST	1.92E−07	0.23	0.3	0.85	20
LR01-9-POST	1.42E−07	0.19	0.31	0.42	29
LR02-15-POST	1.70E−07	0.15	0.12	0.61	25
LR02-30-POST	1.70E−07	0.19	0.17	0.37	31
LR03-15-POST	1.79E−07	0.41	<0.01	0.83	20
LR04-15-POST	1.00E−07	0.47	0.33	<0.1	>40
LR04-30-POST	1.82E−07	0.49	0.13	0.16	38
LR05-15-POST	1.61E−07	<0.01	<0.01	0.59	25
LR05-30-POST	1.96E−07	<0.01	<0.01	<0.1	>40
LR05-9-POST	1.42E−07	<0.01	0.3	0.87	19
LR07-15-POST	1.01E−07	<0.01	<0.01	1.12	14
LR07-30-POST	1.45E−07	0.2	0.11	0.19	37
LR09-21-POST	1.01E−07	<0.01	0.63	1.2	12
LR09-30-POST	1.17E−07	0.53	0.61	0.3	32
LR09-45-POST	1.43E−07	0.6	0.9	0.37	31
LR09-9-POST	1.01E−07	0.18	1.01	<0.1	>40
LR10-15-POST	1.94E−07	<0.01	0.13	0.45	29
LR10-21-POST	1.14E−07	<0.01	0.13	0.76	21
LR10-30-POST	1.53E−07	<0.01	0.19	0.16	38
LR10-9-POST	2.14E−07	0.52	1.52	1.1	14
LR12-24-POST	2.50E−07	0.56	0.65	<0.1	>40
LR12-30-POST	2.65E−07	0.51	0.48	0.24	35
LR13-30-POST	6.23E−08	<0.01	0.3	<0.1	>40

SF_6 is used quantitatively to estimate SF_6-based piston flow ages, simply representing elapsed time between sampling and the last contact with atmosphere, assuming no mixing. SF_6 piston flow ages are broadly associated with the with more complex, derived ^{3}H-^{3}He model ages (Fig. 5; *t(9) = 1.9; p = 0.09 for SF_6 ages < 40 years and*

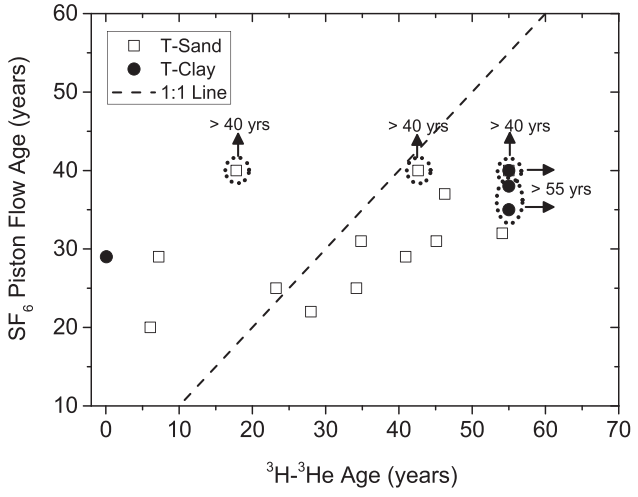

Fig. 5. SF_6 age, representing a "piston flow" age with no mixing, *versus* independently determined ^{3}H-^{3}He model ages in groundwater from T-Sand (open square) and T-Clay (filled circle) with a 1:1 line (dashed). Symbols circled with a dotted line indicate that they exceed the quantifiable age range of the dating technique; *e.g.* >55 years for ^{3}H-^{3}He ages or >40 years for SF_6 ages.

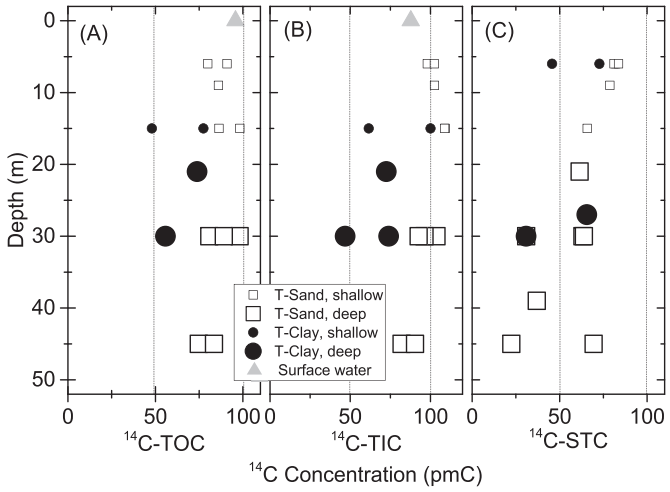

Fig. 6. Depth profiles of (A) ^{14}C-TOC concentrations (aqueous), (B) ^{14}C-TIC concentrations (aqueous, uncorrected) and (C) ^{14}C-STC concentrations for sites along T-Sand (open square) and T-Clay (filled circle) and surface water (surface waters represented at 0 m depth). Depth distinctions are <20 m for shallow and >20 m for deep. The analytical uncertainties in ^{14}C lie within the larger symbols shown.

^{3}H-^{3}He ages < 55 years), with a slight bias towards younger groundwater ages with the SF_6 model. This quantitatively and independently confirms a dominant young component in the groundwaters, supports minimal mixing in most samples, and suggests minimal impact of mantle He and/or other interferences on the derived ^{3}H-^{3}He ages. The strong relationship of SF_6 piston flow ages with depth ($t(19) = 4.4$; $p < 0.05$, *for SF_6 ages < 40 years*) further confirms a strong overall vertical hydrological control in the study area. Potential terrigenic production of SF_6 in sedimentary aquifers (Darling et al., 2012; von Rohden et al., 2010; Friedrich et al., 2013) is expected to be minimal in this study area, given the geological setting, the strong correlation of SF_6 age and depth, and that anomalously high concentrations of SF_6 were not observed. The derivation of CFC and SF_6-based mixing models to determine flow regimes within the study area is the subject of ongoing work by co-authors.

3.4. Bulk radiocarbon groundwater total organic carbon (^{14}C-TOC), total inorganic carbon (^{14}C-TIC) and sedimentary total carbon (^{14}C-STC) concentrations

The bulk radiocarbon total organic carbon (^{14}C-TOC) concentration of groundwater is compared to the bulk sedimentary total carbon (^{14}C-STC) and groundwater total inorganic carbon (^{14}C-TIC) concentrations (Fig. 6 for overall data; Fig. 7 for site-specific profiles at major well clusters). The ^{14}C-TOC groundwater concentrations vary greatly from ~48 to 98 pmC (corresponding to an age of ~<150 years to ~6000 years). The highest ^{14}C-TOC concentrations occur near rapid recharge zones (*e.g.* LR05 and LR01) and provide evidence that relatively young, surface-derived OM can be transported into aquifers at depth under natural recharge conditions, especially near sand-dominated areas or ponds. There are no statistically significant relationships between ^{14}C-TOC or ^{14}C-TIC across the overall study area (Fig. 6A & B), although localized trends are observed (*e.g.* ^{14}C-TIC decreases with depth at LR10 and LR14 as shown on Fig. 7D & E). Sedimentary ^{14}C-STC generally decreases with depth throughout the study area, as would be generally expected in deltaic settings (Fig. 6C; $t(14) = -3.1$, $p < 0.05$).

Comparisons of paired groundwater ^{14}C-TOC and surrounding sedimentary ^{14}C-STC concentrations reveal two relationships: (A) ^{14}C-TOC is greater than ^{14}C-STC concentration (~88% of paired samples), requiring contributions from modern, surface derived OM or younger sedimentary organic matter (SOM) transported from upstream (Lawson et al., 2013); and (B) ^{14}C-TOC is less than ^{14}C-STC concentration (~12% of paired samples) which implies a contribution from older SOM. This second relationship was only observed at one location (LR01-6) and although values are within ~3 pmC, could plausibly be explained given that the sample is very shallow and within the zone of seasonal water level fluctuations (Richards et al., 2017a) which could potentially transport OM upwards from slightly greater depths within the subsurface during the monsoon season. As most samples are modern (*e.g.* ^{3}H-active and contain SF_6/CFCs), and the TOC is older than the transporting water, a contribution from older SOM is required (Lawson et al., 2013), which is further supported because ^{3}H-^{3}He and SF_6 signatures indicate limited groundwater mixing. ^{14}C-TIC confirms a modern component of recharge in some areas, particularly near rapid recharge zones along T-Sand and in shallow samples.

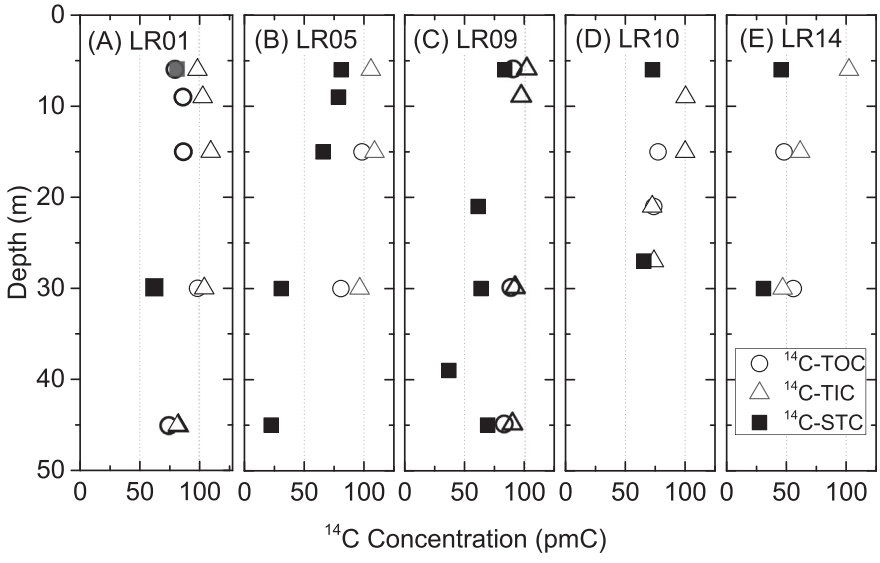

Fig. 7. Radiocarbon total organic carbon (aqueous) (^{14}C-TOC, open circles, ranging from ~48–98 pmC corresponding to an age of ~140–6000 yrs. BP), total inorganic carbon (aqueous) (^{14}C-TIC, open triangles, ranging from ~47–110 pmC corresponding to modern −~3900 yrs. BP, uncorrected); and sedimentary total carbon (^{14}C-STC, filled squares, ranging from ~22–84 pmC corresponding to an age of ~1430–12,000 yrs. BP) concentration depth profiles for T-Sand clusters (A) LR01; (B) LR05; and (C) LR09, and T-Clay clusters (D) LR10 and (E) LR14. Errors in ^{14}C concentration lie within the symbols shown.

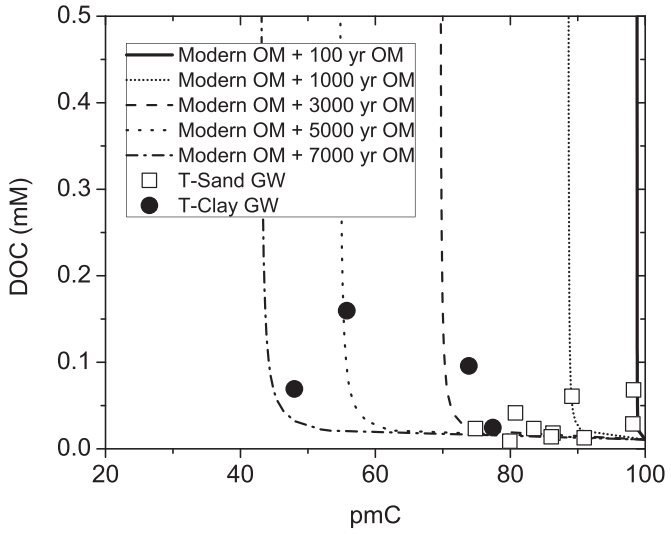

Fig. 8. ^{14}C-TOC groundwater from T-Sand (open squares) and T-Clay (filled circles) and the modelled evolution in the age of bulk DOC through the mixing of sedimentary OM and modern OM (Lawson et al., 2013). Measured ^{14}C-TOC concentrations are compared with model concentrations of DOC calculated based on two-component mixing of 0.002 mM of modern OM with sedimentary OM with ages of 100, 1000, 3000, 5000 and 7000 years. Mixing profiles demonstrate the requirement for contributions of modern DOC and place upper limits on the age of sedimentary OM contributions of 7000 years. The analytical uncertainties in pmC lie within the symbol shown.

Measured groundwater ^{14}C-TOC concentrations are consistent with mixing of 0.002 mM of modern DOC with SOM between ~38 and 99 pmC (~100–8000 years old; Fig. 8). The majority of groundwaters are consistent with mixing with SOM concentrations between ~70 and 89 pmC (~1000 and 3000 years old), supporting postulations of near-surface sedimentary OM driving arsenic release (Lawson et al., 2013; Polizzotto et al., 2008; Kocar et al., 2008). In other limited cases, mixing is consistent with contributions from (i) very modern SOM > ~89 pmC (<1000 years old); or (ii) SOM between ~43–55 pmC (~5000 and 7000 years, typical of shallow peat deposits in alluvial floodplains (McArthur et al., 2004)) Notably, all samples from T-Sand are consistent with mixing with <3000 year old SOM, whereas the T-Clay samples indicate older SOM inputs. Estimates of the maximum relative contribution of SOM to the total OM pool range from 2% to 95% (Lawson et al., 2013) (Table 2), with groundwater from T-Clay typically having higher contributions of SOM than T-Sand. This is consistent with slower flow rates and plausibly increased water-sediment interactions in low permeability, clay-dominated areas.

Although subsurface inputs may involve multiple sources, the ^{14}C data indicates that the majority of the subsurface-sourced DOC inventory must derive from shallow sediments. It is important to emphasize that all ^{14}C measurements reported here represent the bulk carbon pool. The bulk organic carbon pool, in particular, is a complex mixture of components deriving from plant, animal and microbial OM sources, all of which are highly variable in structure, composition and bioavailability (McKnight et al., 1992; Thurman, 1985; Benedetti et al., 1996; Hudson et al., 2007). Detailed characterization of the aqueous OM pool using fluorescence spectroscopy (Richards et al., under review) showed a general dominance of terrestrial humic and fulvic-acid like components, with relatively small microbially-derived contributions. Groundwater from T-Sand typically comprises of an OM pool with lower tryptophan-like, fulvic-like and humic-like components and which is less bioavailable as compared to groundwater from T-Clay (Richards et al., under review). Detailed lipid analysis of sediments from the same area indicated that the concentration and type of OM is related to grain size, with clay containing mostly immature, plant-derived SOM and thermally mature SOM in the sands (Magnone et al., 2017). The degree of oxidation of SOM is strongly related to stratigraphy, with older, bound SOM more oxidized than younger SOM (Magnone et al., 2017). The ^{14}C-based mixing models presented here (Table 2) which show that T-Sand groundwater has greater inputs from modern OM as compared to T-Clay with greater inputs from SOM, is consistent with the more detailed organic characterization published elsewhere (Magnone et al., 2017; Richards et al., under review).

3.5. Implications on arsenic mobilization

Arsenic concentrations were linked to ^{3}H-^{3}He ages and are typically lower in shallow, very young waters and increase in deeper, older waters (Fig. 9). The relationship of arsenic with ^{3}H-^{3}He ages allows for a calculation, using linear regression, of an overall arsenic accumulation rate of 0.08 ± 0.03 $\mu M \cdot yr^{-1}$ *(6.3 ± 2.6* $\mu g \cdot L^{-1} \cdot yr^{-1}$*; t (24) = 2.4; p < 0.05 for ^{3}H-^{3}He ages <55 years)*. Site-specific arsenic accrual rates (Table 3) are highly heterogeneous, even along the same transect, and range from 0.09 ± 1.4 $\mu M \cdot yr^{-1}$ *(t(3) = 0.64, p > 0.05)* at site LR09 to 0.55 ± 0.05 $\mu M \cdot yr^{-1}$ *(t(2) = 12.2, p < 0.05)* at site LR05. This heterogeneity indicates, in some circumstances, that arsenic can accumulate much more rapidly than previously considered in Cambodia (Polizzotto et al., 2008), and suggests the contribution of both in-aquifer and near-surface processes in arsenic mobilization. Although

Table 2
Percentage contributions of sedimentary OM and modern surface derived OM. Scenarios A, B and C represent two-component mixing of modern OM with sedimentary OM which is 1000, 6000 and 12,000 years old respectively, representing the range of actual sedimentary carbon age measured (Magnone et al., 2017). Where values are not given the ages of the sedimentary OM that is mixed is younger than the sample and the model does not converge.

Sample ID	SUERC Code (Magnone et al., in review)	^{14}C-TOC Age (Magnone et al., in review)	^{14}C-TOC (Magnone et al., in review)	Sedimentary OM (%)			Modern OM (%)		
		(yrs BP)	(pmC)	A	B	C	A	B	C
LR01-15-PRE	SUERC-56895	1179 ± 35	86.34	–	26	18	–	74	82
LR01-30-PRE	SUERC-57663	148 ± 37	98.18	16	4	2	84	96	98
LR01-45-PRE	SUERC-57670	2328 ± 38	74.84	–	49	33	–	51	67
LR01-6-PRE	SUERC-56905	1798 ± 37	79.94	–	39	26	–	61	74
LR01-9-PRE	SUERC-57669	1204 ± 35	86.08	–	27	18	–	73	82
LR05-15-PRE	SUERC-56900	139 ± 37	98.29	15	3	2	85	97	98
LR05-30-PRE	SUERC-57675	1715 ± 35	80.78	–	37	25	–	63	75
LR09-30-PRE	SUERC-56896	924 ± 37	89.14	95	21	14	5	79	86
LR09-45-PRE	SUERC-57673	1449 ± 38	83.50	–	32	22	–	68	78
LR09-6-PRE	SUERC-57664	760 ± 35	90.97	79	18	12	21	82	88
LR10-15-PRE	SUERC-56903	2056 ± 37	77.42	–	44	29	–	56	71
LR10-21-PRE	SUERC-57690	2434 ± 35	73.86	–	51	34	–	49	66
LR14-15-PRE	SUERC-56906	5897 ± 37	48.00	–	–	68	–	–	32
LR14-30-PRE	SUERC-57666	4692 ± 37	55.76	–	86	58	–	14	42

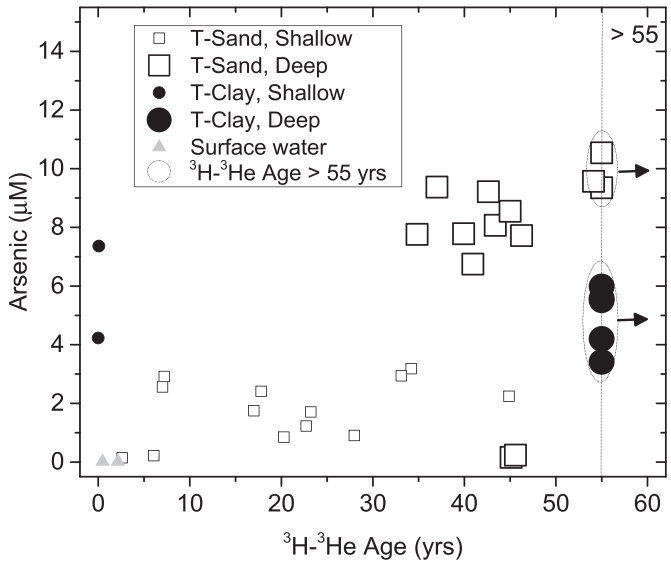

Fig. 9. Arsenic concentration *versus* apparent groundwater ^{3}H-^{3}He age (2014 basis). An overall arsenic loading rate as given by linear regression is 0.08 ± 0.03 μM·yr^{-1} *(t(24) = 2.4; p < 0.05)*. Waters in the dashed circle are >55 years old and were excluded from loading calculations. Errors in ^{3}H-^{3}He and ^{14}C ages lie within the symbols shown.

this heterogeneity is attributed in part to changes in lithology giving rise to rapid recharge zones (Richards et al., 2018; Uhlemann et al., 2017), differences in the composition of the OM pool also vary between sites, and especially between sand and clay-dominated sequences (Richards et al., under review). Isolated contributions to the OM pool from ponds, particularly near site LR05 and LR14, may also contribute to the arsenic loading observed (Lawson et al., 2013; Lawson et al., 2016). Arsenic accumulation is also very rapid at site LR10, where the 15 m sample had a ^{3}H-^{3}He age on the order of only several months, a similar age to the Mekong River (located ~500 m away) and which provides strong evidence that this site is likely within the sphere of surface-groundwater influence originating from monsoonal-driven variations in water level (Benner et al., 2008; Richards et al., 2017a). This seems reasonable particularly given estimations of horizontal flow velocities of around 40 to 170 m·yr^{-1}, with faster velocities conceptually possible in apparent "fast-track" zones. Very young groundwater containing high arsenic may reflect either hydrologic transport of arsenic from modern upstream sources or a rapid removal of oxidants during recharge, leading to developing the reducing conditions required for arsenic mobilization (Lawson et al., 2016). Observed arsenic loading rates are broadly consistent with previously published release rates between ~0.28 ± 0.05 and 0.31 ± 0.08 μM·yr^{-1} (21 ± 4 and 23 ± 6 μg·L^{-1}·yr^{-1} (Radloff et al., 2007), respectively) for incubation experiments with Bangladeshi sediment and groundwater (Radloff et al., 2007), as well as with ^{3}H-^{3}He-derived rates between ~0.26 ± 0.03 and 0.32 ± 0.04 μM·yr^{-1} (19.4 ± 1.9 and 23.8 ± 2.3 μg·L^{-1}·yr^{-1} (Stute et al., 2007), respectively) in Bangladesh (Stute et al., 2007).

The relationship between arsenic and both ^{3}H and SF_6 shows distinct groupings with very high arsenic concentrations observed in young (*e.g.* relatively high ^{3}H and SF_6), old (*e.g.* relatively low ^{3}H and SF_6), shallow and deep groundwaters alike (Fig. 10) (note groupings are defined by ^{3}H rather than ^{3}H-^{3}He age to avoid the ambiguity when ^{3}H-^{3}He age >55 years). These groupings are further discriminated by apparent ^{3}H-^{3}He age, $^{4}He_{rad}$, Eh, DOC and the fluorescent aqueous bulk OM bioavailability proxy β:α (Richards et al., under review) (Table 4). Group 1, characterized by ^{3}H-active groundwaters with relatively low arsenic (0.1–0.2 μM) on T-Sand, also has the lowest DOC, the least reducing conditions and moderate β:α for this study area. Group 2, which is ^{3}H-dead groundwaters (>55 years in ^{3}H-^{3}He age) with moderate/high arsenic (3.2–6.2 μM), contains samples exclusively of deep groundwaters in T-Clay, located relatively near a pond, and is also characterized by high DOC concentrations and relatively high OM bioavailability. The high arsenic in this area may be influenced by pond-derived OM and is consistent with previous work (Lawson et al., 2013; Lawson et al., 2016), including notably high sulfate and dissolved oxygen concentrations (Richards et al., 2017a). Groups 3 and 4 both contain ^{3}H-active groundwaters with high arsenic (0.8–4.4 μM and 6.8–11.1 μM for Group 3 and 4, respectively), reducing conditions and similar concentrations of DOC and β:α, predominantly along T-Sand. The dominant segregation between these groups is depth, with Group 4 containing higher arsenic and deriving from deeper (>20 m) within the aquifer sands. Importantly, the fact that some shallow and deep groundwaters in both of these groups have very high arsenic and are very young indicates that arsenic mobilization and accumulation is occurring very rapidly in these areas. Deeper waters typically have higher arsenic, which is consistent with Fig. 9. The mobilization and accumulation of arsenic in all modern groundwater samples falling on the input curves for tritium (Fig. 3C) and SF_6 must occur on the maximum timescale of several decades.

Relationships between arsenic, arsenic accumulation rates, β:α and ^{14}C-TOC age (Fig. 11) also reflect distinct trends and differences between transects. In several cases very high concentrations of arsenic (*e.g.* ~3–8 μM, respectively) are found in samples containing very young ^{14}C-TOC (*e.g.* <150 years) (Fig. 11A) in rapid recharge zones, suggesting that arsenic accumulation is not exclusively a slow build-up over hundreds or thousands of years (Polizzotto et al., 2008; Benner et al., 2008; Kocar et al., 2014). All of the samples containing arsenic concentrations > 5 μM have ^{14}C-TOC ages of ~2000 years or less, notably with the ^{14}C-TOC being much older in the T-Clay than in T-Sand transect. Arsenic accumulation rates, derived on the basis of both ^{14}C-TOC age (Fig. 11B) and groundwater ^{3}H-^{3}He age (Fig. 11C), are highly variable, site/transect specific and are inversely proportional to ^{14}C-TOC age, with the arsenic accumulating at the fastest rates in young groundwater containing young TOC on T-Sand. The relatively slow accumulation of arsenic over time, particularly on T-Clay, is consistent with models suggesting that slow recharge through surficial clays results in extensive arsenic accumulation (Polizzotto et al., 2008; Kocar et al., 2014).

Accumulation rates derived from ^{14}C-TOC and ^{3}H-^{3}He ages inherently reflect different processes, with ^{14}C-TOC-derived rates

Table 3
Arsenic loading and correlation statistics as calculated by linear regression between arsenic and ^{3}H-^{3}He age for groundwater <55 years ^{3}H-^{3}He age; (i) a loading for T-Clay is not provided because samples >55 years were almost entirely from this transect and (ii) LR10 calculations only include the 15 m depth sample giving rise to very high apparent loading at this site.

Site	As loading (μM·yr^{-1})	As loading (μg·L^{-1}·yr^{-1})	Standard error (%)	Degrees of freedom	t-value	p-Value	N > 55 years
LR01	0.14	10	35	6	2.9	0.03	2
LR02	0.38	29	21	2	4.8	<0.01	0
LR05	0.55	41	8	2	12.2	0.01	0
LR07	0.28	21	13	1	7.3	0.09	0
LR09	0.09	7	160	3	0.6	0.57	0
LR10	43	3190	n/a	0	n/a	n/a	2
T-Sand	0.13	10	29	22	3.5	<0.01	2
Overall	0.08	6	41	24	2.4	0.03	8

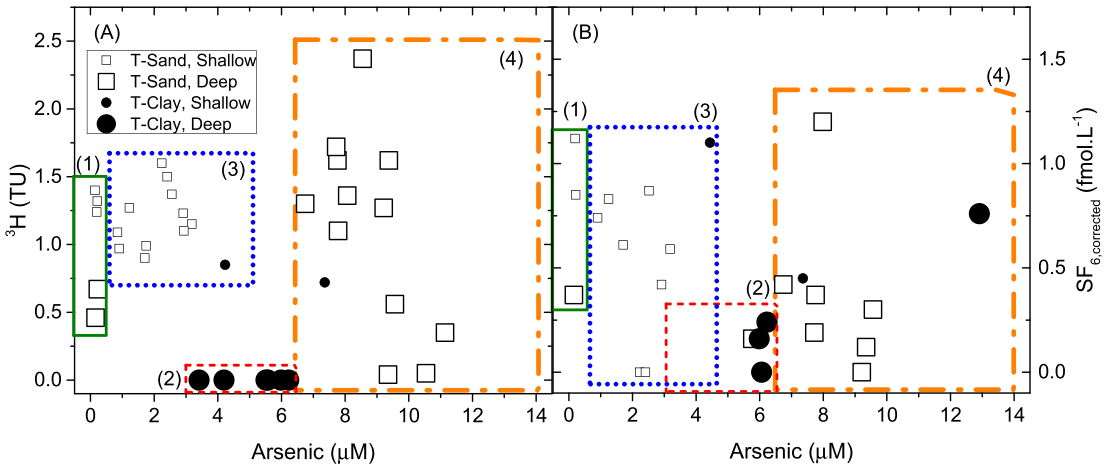

Fig. 10. Groups of groundwaters discriminated by (A) ^{3}H and arsenic: (1) ^{3}H-active groundwaters with low arsenic (0.1–0.2 μM; indicated by green solid box); (2) ^{3}H-dead groundwaters with high arsenic (3.2–6.2 μM; indicated by dashed red box) exclusive to T-Clay; (3) shallow (<20 m), ^{3}H-active groundwaters with moderate arsenic (0.8–4.4 μM; indicated by dotted blue box); and (4) predominately deep (>20 m), ^{3}H-active groundwaters with very high arsenic (6.8–11.1 μM; indicated by dash-dotted orange box). Shallow groundwaters are from <20 m depth; deep groundwaters are from >20 m depth. The maximum error in ^{3}H is approximately ±0.2 TU, with most within ±0.1 TU. Similar groupings are observed with (B) SF_6 and arsenic, with high arsenic groundwaters containing a wide range of SF_6 concentrations and associated piston flow ages (Table 1).

Table 4
Further characterization of groupings as discriminated by ^{3}H and As, with apparent ^{3}H-^{3}He age, $^4He_{rad}$, Eh, DOC and fluorescent organic matter bioavailability indicator β:α (pre-monsoon only (Richards et al., under review)) (all shown as ranges).

Group	As (μM)	^{3}H (TU)	^{3}H-^{3}He age (yrs)	$^4He_{rad}$ (ccSTP·kg^{-1})	Eh (mV)	DOC (mg·L^{-1})	β:α	Zone
1	0.1–0.2	0.7–1.4	3–45	0–0.3·10^{-5}	−110–10	0.8–3.7	0.56–0.64	Sandy, mixed depth
2	3.2–6.2	0.0	>55	0–1.9·10^{-5}	−170–30	3.9–15	0.58–0.69	Clay, deep
3	0.8–4.4	0.9–1.6	0–45	0–2.5·10^{-5}	−170–30	0.9–6.8	0.54–0.63	Sandy, shallow
4	6.8–11.1	0.1–2.4	0–>55	0–1.2·10^{-5}	−160–−20	2.2–6.7	0.53–0.63	Sandy, deep

representing accumulation relative to the aquifer system bulk OM, which inherently (i) represent many sources of differing relative importance in arsenic mobilization and/or accumulation; (ii) do not necessarily follow groundwater flowpath evolution; (iii) assume that bulk TOC represents the only electron donor source for arsenic release; and (iv) represent a mean overall rate, even though TOC could undergo the majority of its transformation relatively quickly after deposition, particularly in tropical settings. In contrast, the ^{3}H-^{3}He-derived rates reflect the actual groundwater residence time but give no indication of TOC inputs. Despite these differences, rates derived from both methods show similar trends. The rates on either basis are notably higher in T-Sand than in T-Clay, with the fastest rates from both methods occurring at site LR01 in a rapid recharge zone – with the highest accumulation rate based on ^{14}C-TOC age being in a relatively deep sample (LR01-30,

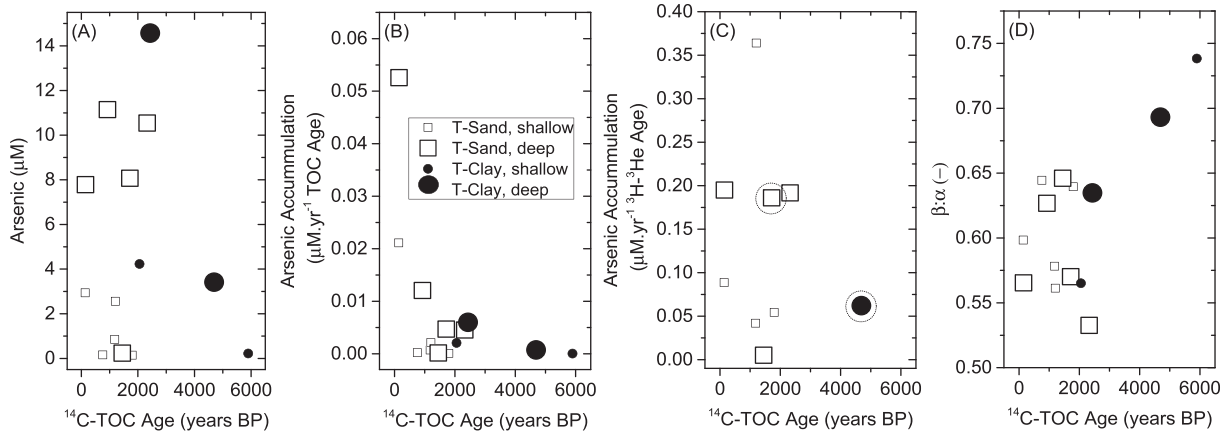

Fig. 11. (A) Arsenic concentration; (B) arsenic accumulation rate on a TOC-age basis (μM·yr^{-1} TOC age, ranging from 3.8 × 10^{-5} μM·yr^{-1} TOC age at LR14-15 to 0.05 μM·yr^{-1} TOC age at LR01-30); (C) arsenic accumulation rate on a groundwater residence time ^{3}H-^{3}He-age basis (μM·yr^{-1} ^{3}H-^{3}He-age, ranging from 0.005 μM·yr^{-1} ^{3}H-^{3}He-age at LR09-45 to 0.36 μM·yr^{-1} ^{3}H-^{3}He-age at LR01-9); and (D) aqueous organic matter bioavailability proxy β:α (–) (Richards et al., under review) *versus* groundwater ^{14}C-TOC age indicating distinct differences between T-Sand (open squares) and T-Clay (filled circles). Analytical uncertainties in ^{14}C-TOC age would appear within the symbol shown. Circled/dashed data points (n = 2) on (C) show where ^{3}H-^{3}He age is >55 years and thus rates represent a maximum rate. "Shallow" and "deep" refer to <20 m and >20 m in depth, respectively.

0.05 μM·yr^{-1} TOC age) whereas the highest accumulation based on groundwater age is in the shallow sample at the same site (LR01-9, 0.36 μM·yr^{-1} ^{3}H-^{3}He-age). Further, the several samples with high arsenic accumulation rates ~0.2 μM·yr^{-1} ^{3}H-^{3}He-age (Fig. 11C) are also located at LR01 (30 and 45 m depths) and LR05-30. Previous characterization of sedimentary OM indicated the presence of thermally mature derived (sedimentary) organic carbon in sand-dominated sequences in this study area (Magnone et al., 2017), which perhaps offers an explanation for the observed trends.

Such local point source contributions from rapid recharge zones are likely to control the bulk aquifer geochemistry. This is particularly important for example along T-Clay, where the inferred recharge rates suggest a layered, multi-porosity domain. The resulting aquifer geochemistry (including arsenic concentration) will thus reflect a composite effect of the rate of biogeochemical arsenic release, diffusive contributions (likely driving arsenic from low conductivity zones into high conductivity zones) plus other processes which affect net accumulation such as sorption/desorption (Goldberg et al., 2007; Peters, 2008; Javed et al., 2013; Mai et al., 2014; Diwakar et al., 2015; Yang et al., 2015; Casanueva-Marenco et al., 2016; Richards et al., under review). The relative importance of those inputs will depend upon the flow rate, and thus will depend on lithology amongst other hydrological controls, and would be expected to vary widely across the study area, given the heterogeneous and localized recharge rates.

This data also suggests that the arsenic accumulation rates are highest near the surface, at some locations (*e.g.* LR01), and importantly that the rates are not necessarily sustained throughout vertical groundwater flow paths. For example given the rate of 0.36 μM·yr^{-1} ^{3}H-^{3}He-age observed at LR01-9, the projected arsenic concentration at >55 years (the ^{3}H-^{3}He age of LR01-45, the 45 m sample at the same site) would be >19.8 μM purely on the basis of age estimation; however, the actual measured arsenic concentration at LR01-45 is only 10.5 μM. That the maximum arsenic accumulation rates do not appear to be sustained across the flow path indicates that other processes must also be influencing the observed trends, particularly including sorption/desorption and/or complex partial equilibrium conditions (Goldberg et al., 2007; Peters, 2008; Javed et al., 2013; Mai et al., 2014; Diwakar et al., 2015; Yang et al., 2015; Casanueva-Marenco et al., 2016; Richards et al., under review) which may also be influenced by seasonally shifting groundwater gradients (Benner et al., 2008; Richards et al., 2017a) as well as presence of other groundwater and sedimentary constituents. Further, co-occurring processes such as methanogenesis can also lead to a substantial consumption of organic carbon (Postma et al., 2016), with significant concentrations of methane being measured in selected samples (Richards et al., under review). In other cases, lithological impacts might also impact arsenic accumulation and in-aquifer transport; for example on the basis of the observed accumulation rate at LR09-9 (0.05 μM·yr^{-1} ^{3}H-^{3}He-age) the projected concentration at LR09-45 would be 2.2 μM based on age; however observed arsenic at LR09-45 is only 0.005 μM. This particular case can plausibly be explained by a clay lens occurring ~40 m in depth at that site; similar localized impacts are likely to occur in other locations as well. One further contrasting example is at site LR05, where apparent accumulation at LR05-30 (0.19 μM·yr^{-1} ^{3}H-^{3}He-age) is actually higher than that of the shallower sample at LR05-15 (0.09 μM·yr^{-1} ^{3}H-^{3}He-age); in this case there is evidence of continued in-aquifer arsenic mobilization, noting that this site is very near a pond which could introduce pond-derived OM into the aquifer. Particularly relevant to this interpretation may be geomorphological features such as point-bar and/or oxbow lakes/clay-plugs, which have been proposed to impact the migration and accumulation of released arsenic, particularly due to permeability differences, in other shallow, circum-Himalayan groundwaters (Donselaar et al., 2017). The high arsenic release rates observed in both shallow and deep groundwater supports that arsenic can plausibly be mobilized over the entire length of the groundwater flow paths, although net accumulation rates can vary significantly and are also potentially

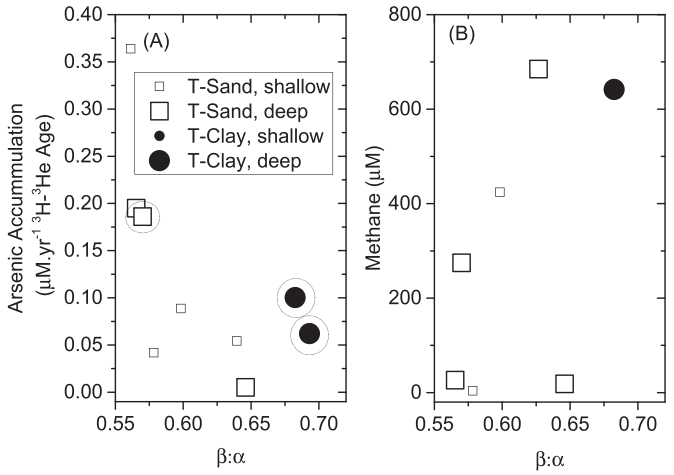

Fig. 12. (A) Arsenic accumulation rate on a groundwater residence time ^{3}H-^{3}He-age basis (μM·yr^{-1} ^{3}H-^{3}He-age) and (B) methane concentration for selected samples (Richards et al., under review) *versus* the aqueous bulk organic matter bioavailability proxy β:α (–) (Richards et al., under review) for T-Sand (open squares) and T-Clay (filled circles). Circled/dashed data points (n = 3) on (A) show where ^{3}H-^{3}He age is >55 years and thus rates represent a maximum rate. "Shallow" and "deep" refer to <20 m and >20 m in depth, respectively.

impacted, to varying degrees, by a number of confounding processes including sorption/desorption and/or methanogenesis, as well as other geochemical, hydrological and/or geomorphological controls.

Interestingly, a significant positive correlation exists between the bulk OM bioavailability proxy β:α and ^{14}C-TOC age (Fig. 11D, $t(12) = 3.13$, $p < 0.01$); this shows that in this setting, the bulk aqueous OM is more bioavailable in groundwater containing older OM in clay-dominated sequences rather than in groundwater containing young OM. However, these older ^{14}C-TOC ages also usually have lower concentrations of arsenic and lower arsenic accumulation rates, as discussed previously (Fig. 11A–C). The important extension of this argument is the relationship between ^{3}H-^{3}He derived arsenic accumulation rates and β:α (Fig. 12A), which are broadly inversely correlated ($t(8) = -2.22$, $p = 0.06$, *note* $p > 0.05$). This means that the highest rates of arsenic accumulation are found where β:α is lowest (*e.g.* where bulk DOM is least bioavailable), which is also where methane concentrations are lowest (Fig. 12B) (Richards et al., under review). This has several possible interpretations, including that bulk OM bioavailability is not a sufficient proxy to predict arsenic release/accumulation (which could suggest that there are other, more dominant contributors including specific organic compounds or other inorganic proxies; or that bulk OM bioavailability does not necessarily represent OM which is bioavailable to the organisms which are involved in arsenic mobilization), that methanogenesis is occurring in highly bulk bioavailable locations (*e.g.* in clay dominated sequences) which can lead to a substantial consumption of organic carbon (Postma et al., 2016), limiting its available for reductive dissolution of arsenic bearing iron minerals, and/or the presence of other dominant processes. These are interesting possibilities and further work is required to disentangle these potential confounders.

4. Conclusions

Using a complementary suite of geochemical tracers (including ^{14}C, ^{3}H, ^{3}He, ^{4}He, Ne, δ^{18}O, δD, CFCs and SF_6) to study the evolution of groundwater geochemistry along dominant flow paths in a heavily arsenic-impacted aquifer in Cambodia, there is substantial evidence modern groundwater and OM transport to depths >30 m. However, despite this, evidence from ^{14}C-TOC and EEM suggests that the older bulk OM in clay-dominated sequences is more bioavailable to the indigenous microbial community than bulk OM in younger and sand-dominated sequences. A strong relationship between modern age tracers and depth

($p < 0.01$ for ^{3}H-^{3}He age) indicate a dominant vertical hydrological control in the study area. The relationships between age-related tracers and arsenic allow for estimations of groundwater arsenic accumulation rates which are highly heterogeneous and particularly high in rapid recharge zones especially in sandy areas. Such local point source contributions from rapid recharge zones are postulated to introduce surface derived OM, leading to more rapid in-aquifer arsenic mobilization and influencing bulk groundwater geochemistry throughout the aquifer. These data also provide evidence that near-surface wetland sediments control the slow build-up of arsenic in lower permeability areas. Evidence for the dual role of surface-derived and near-surface OM begins to reconcile a number of previous studies (Lawson et al., 2013; Lawson et al., 2016; Polizzotto et al., 2008; Kocar et al., 2008; Magnone et al., 2017) and the co-occurrence of processes is attributed to the natural heterogeneity of the subsurface.

High arsenic concentrations were observed in both shallow and deep groundwater, suggesting that arsenic can plausibly be mobilized over the entire length of the groundwater flow paths, although net accumulation rates vary significantly. Apparent groundwater arsenic accumulation rates are, in most cases, highest near the surface, perhaps reflecting the proximity to the redox cline or the characteristics of the OM pool, and may be impacted by a number of confounding processes during transport along groundwater flow paths (*e.g.* continued in-aquifer arsenic mobilization, sorption/desorption, methanogenesis) and other geochemical and/or hydrological controls. Aspects of the results obtained here are broadly consistent with other studies conducted within the region (*e.g.* in Cambodia, Vietnam, Bangladesh) (Islam et al., 2004; Bhattacharya et al., 1997; van Geen et al., 2004; Postma et al., 2007; Rowland et al., 2009; Aggarwal et al., 2000; Harvey et al., 2002; van Geen et al., 2003; Lawson et al., 2008; Sengupta et al., 2008; van Dongen et al., 2008; McArthur et al., 2011; Neumann et al., 2011; Lawson et al., 2013; Lawson et al., 2016; Datta et al., 2011; Nickson et al., 1998; McArthur et al., 2001; McArthur et al., 2004; Polizzotto et al., 2008; Kocar et al., 2008; Papacostas et al., 2008; Neumann et al., 2010; Rowland et al., 2007; Al Lawati et al., 2012; Al Lawati et al., 2013; Magnone et al., 2017; Lawrence et al., 2000; Aggarwal et al., 2003; Harvey et al., 2003; Mailloux et al., 2013; van Geen et al., 2008; Radloff et al., 2017; Schaefer et al., 2016; Stuckey et al., 2016; Gault et al., 2005; Neumann et al., 2009; Fendorf et al., 2010; Mladenov et al., 2010; Neumann et al., 2014; Polya and Charlet, 2009), as detailed in the discussion and suggests that such aquifers may be particularly vulnerable to anthropogenic interferences, such as groundwater pumping and sediment excavation.

Acknowledgements

This research was funded by a United Kingdom Natural Environmental Research Council (NERC) Standard Research Grant (NE/J023833/1 to DP, BvD and CB) with additional support from a NERC PhD studentship (NE/L501591/1 to DM) and a Leverhulme Trust Early Career Fellowship (ECF2015-657 to LR), both at the University of Manchester, and a NERC Collaborative Awards in Science and Engineering studentship (NE/EEA6549/1 to LC) at Lancaster University under the supervision of Greg Holland, Andrew Binley and DCG. Radiocarbon analysis was supported by the NERC Radiocarbon Facility NRCF010001 (allocation numbers 1814.0414, 1834.0714 and 1906.0415). Stable isotope analysis was conducted at SUERC and was supported by a NERC Isotope Geosciences Facilities Access grant IP-1505-1114. The following people are gratefully acknowledged for their excellent contributions to the field campaigns: Chivuth Kong, Pheary Meas, Yut Yann and Teyden Sok (all Royal University of Agriculture, Phnom Penh, Cambodia); Chhengngunn Aing, Zongta Sang, Vichet Hang, Sereyrath Aing, Borey Horm, Savuth Yim and Sitha Sean (all Royal University of Phnom Penh); Helen Downie and Emma Naden (The University of Manchester, UK); Lucy Oxby (formerly British Geological Survey, UK); and Kheng Sok (2 World Travel, Cambodia). Ann Hall, Marc Hall, Lori Frees, Lori Allen, Dina Kuy, the late Mickey Sampson and others (all Resources Development International – Cambodia, RDI) are thanked for logistical support and the usage of laboratory facilities at RDI. Paul Lythgoe, Alastair Bewsher, Ahmed Ali Nassir Al Bualy (all The University of Manchester), Maria Casanueva-Marenco (Cádiz University, Spain) and Francis Elliott (NERC Radiocarbon Facility, UK) are thanked for analytical support. Dan Lapworth and Peter Williams (British Geological Survey, Wallingford, UK) are thanked for assistance with fluorescence measurements/interpretation. Xiaomei Xu (Keck Carbon Cycle AMS Facility, University of California Irvine, USA) is thanked for ^{14}C-TOC small sample analysis and staff at the SUERC AMS Laboratory for all other ^{14}C analysis. Merren Jones and Greg Holland (both The University of Manchester) are thanked for useful discussions as is Michael Lawson (formerly University of Manchester) for his contributions to ideas underpinning this work. Finally, this research would not have been possible without the support of the local drilling team led by Hok Meas and local landowners. The views expressed here do not necessarily represent those of the institutions, funders or individuals whose support is acknowledged.

References

Aeschbach-Hertig, W., et al., 2008. Modeling excess air and degassing in groundwater by equilibrium partitioning with a gas phase. Water Resour. Res. 44, W08449.
Aggarwal, P.K., et al., 2000. Isotope Hydrology of Groundwater in Bangladesh: Implications for Characterization and Mitigation of Arsenic in Groundwater. International Atomic Energy Agency, Vienna (I.-T.P.R. BGD/8/016 editor.).
Aggarwal, P.K., Basu, A.R., Kulkarni, K.M., 2003. Comment on "Arsenic mobility and groundwater extraction in Bangladesh" (I). Science 300, 584b.
Al Lawati, W.M., et al., 2012. Characterisation of organic matter and microbial communities in contrasting arsenic-rich Holocene and arsenic-poor Pleistocene aquifers, Red River Delta, Vietnam. Appl. Geochem. 27, 315–325.
Al Lawati, W.M., et al., 2013. Characterisation of organic matter associated with groundwater arsenic in reducing aquifers of southwestern Taiwan. J. Hazard. Mater. 262, 970–979.
Andrews, J.N., 1985. The isotopic composition of radiogenic helium and its use to study groundwater movement in confined aquifers. Chem. Geol. 49, 339–351.
Appelo, C.A.J., Postma, D., 1993. Geochemistry, Groundwater and Pollution. Balkema.
Bell, R.A., et al., 2017. A baseline survey of dissolved methane in aquifers of Great Britain. Sci. Total Environ. 601–602, 1803–1813.
Benedetti, M.F., et al., 1996. Metal ion binding by natural organic matter: from the model to the field. Geochim. Cosmochim. Acta 60 (14), 2503–2513.
Benner, S.G., et al., 2008. Groundwater flow in an arsenic-contaminated aquifer, Mekong Delta, Cambodia. Appl. Geochem. 23 (11), 3072–3087.
Benson, B.B., Krause, D., 1980. Isotopic fractionation of helium during solution: a probe for the liquid state. J. Solut. Chem. 9 (12), 895–909.
Beyerle, U., et al., 1999. Infiltration of river water to a shallow aquifer investigated with $^{3}H/^{3}He$, noble gases and CFCs. J. Hydrol. 220, 169–185.
Bhattacharya, P., Chatterjee, D., Jacks, G., 1997. Occurrence of arsenic contaminated groundwater in alluvial aquifers from delta plains, Eastern India: options for safe drinking water supply. Water Resour. Dev. 13, 79–92.
Boutton, T.W., et al., 1983. Comparison of quartz and Pyrex tubes for combustion of organic samples for stable carbon isotope analysis. Anal. Chem. 55, 1832–1833.
Bryant, C.L., et al., 2013. Storage and hydrolysis of seawater samples for inorganic carbon isotope analysis. Radiocarbon 55 (3–4).
Busenberg, E., Plummer, L.N., 2000. Dating young groundwater with sulfur hexafluoride: natural and anthropogenic sources of sulfur hexafluoride. Water Resour. Res. 36 (10), 3011–3030.
Casanueva-Marenco, M.J., et al., 2016. Selective chemical extractions of Cambodian aquifer sediments - evidence for sorption processes controlling groundwater arsenic. Arsenic Research and Global Sustainability: Proceedings of the 6th International Congress on Arsenic in the Environment (Stockholm, Sweden).
Charlet, L., Polya, D.A., 2006. Arsenic in shallow, reducing groundwaters in southern Asia: an environmental health disaster. Elements 2, 91–96.
Clarke, W.B., Jenkins, W.J., Top, Z., 1976. Determination of tritium by mass spectrometric measurement of ^{3}He. Int. J. Appl. Radiat. Isot. 27, 515–522.
Cook, P., Solomon, D., 1995. Transport of atmospheric trace gases to the water table: implications for groundwater dating with chlorofluorocarbons and krypton 85. Water Res. Res. 31 (2), 263–270.
Darling, W.G., Gooddy, D.C., 2006. The hydrogeochemistry of methane: evidence from English groundwaters. Chem. Geol. 229, 293–312.
Darling, W.G., Gooddy, D.C., 2007. Assessing the applicability of global CFC and SF_6 input functions to groundwater dating in the UK. Sci. Total Environ. 387 (1), 353–362.
Darling, W.G., et al., 2012. The practicalities of using CFCs and SF_6 for groundwater dating and tracing. Appl. Geochem. (27), 1688–1697.
Datta, S., et al., 2011. Perennial ponds are not an important source of water or dissolved organic matter to groundwaters with high arsenic concentrations in West Bengal, India. Geophys. Res. Lett. 38, L20404.
Diwakar, J., et al., 2015. Arsenic mobilization in an alluvial aquifer of the Terai region, Nepal. J. Hydrol. Reg. Stud. 4, 59–79.

van Dongen, B., et al., 2008. Hopane, sterane and n-alkane distributions in shallow sediments hosting high arsenic groundwaters in Cambodia. Appl. Geochem. 23, 3047–3058.
Donnelly, T., et al., 2001. Hydrogen isotope analysis of natural abundance and deuterium-enriched waters by reduction over chromium on-line to a dynamic dual inlet isotope-ratio mass spectrometer. Rapid Commun. Mass Spectrom. 15, 1297–1303.
Donselaar, M.E., Bhatt, A.G., Ghosh, A.K., 2017. On the relation between fluvio-deltaic flood basin geomorphology and the wide-spread occurrence of arsenic pollution in shallow aquifers. Sci. Total Environ. 574, 901–913.
Dowling, C.B., Porida, R.J., Basu, A.R., 2003. The groundwater geochemistry of the Bengal Basin: weathering. Chemsorption, and trace metal flux to the oceans. Geochim. Cosmochim. Acta 67 (12), 2117–2136.
Fendorf, S., Michael, H.A., van Geen, A., 2010. Spatial and temporal variations of groundwater arsenic in south and southeast Asia. Science 328, 1123–1127.
Freeman, S.P.T., et al., 2010. Improved SSAMS performance. Nucl. Inst. Methods Phys. Res. B 268, 715–717.
Friedrich, R., et al., 2013. Factors controlling terrigenic SF_6 in young groundwater of the Odenwald Region (Germany). Appl. Geochem. 33, 318–329.
Fulda, C., Kinzelbach, W., 2000. Sulphur Hexafluoride (SF_6) as a New Age-Dating Tool for Shallow Groundwater: Methods and First Results. IAHS Publication, pp. 181–186.
Gault, A.G., et al., 2005. Microcosm depth profiles of arsenic release in a shallow aquifer, West Bengal. Mineral. Mag. 69 (5), 855–863.
van Geen, A., et al., 2003. Comment on "Arsenic mobility and groundwater extraction in Bangladesh" (II). Science 300, 584c.
van Geen, A., et al., 2004. Decoupling of As and Fe release to Bangladesh groundwater under reducing conditions. Part II: evidence from sediment incubations. Geochim. Cosmochim. Acta 68 (17), 3475–3486.
van Geen, A., et al., 2008. Flushing history as a hydrogeological control on the regional distribution of arsenic in shallow groundwater of the Bengal Basin. Environ. Sci. Technol. 42 (7), 2283–2288.
van Geen, A., et al., 2013. Retardation of arsenic transport through a Pleistocene aquifer. Nature 501, 204–207.
Gillispie, E.C., Andujar, E., Polizzotto, M.L., 2016. Chemical controls on abiotic and biotic release of geogenic arsenic from Pleistocene aquifer sediments to groundwater. Environ. Sci. Process. Impact. 18, 1090–1103.
Goldberg, S., et al., 2007. Adsorption-desorption processes in subsurface reactive transport modelling. Vadose Zone J. 6 (3), 407–435.
Gooddy, D.C., Darling, W.G., 2005. The potential for methane emissions from groundwaters of the UK. Sci. Total Environ. 339, 117–126.
Gooddy, D.C., et al., 2006. Using chlorofluorocarbons (CFCs) and sulphur hexafluoride (SF_6) to characterise groundwater movement and residence time in a lowland Chalk catchment. J. Hydrol. 330, 44–52.
Harvey, C.F., et al., 2002. Arsenic mobility and groundwater extraction in Bangladesh. Science 298, 1602–1606.
Harvey, C.F., et al., 2003. Response to comments on "Arsenic mobility and groundwater extraction in Bangladesh". Science 300, 584d.
Hinsby, K., et al., 2007. Transport and degradation of chlorofluorocarbons (CFCs) in the pyritic rabis creek aquifer, Denmark. Water Resour. Res. 43 (10).
Horneman, A., et al., 2008. Degradation rates of CFC_{11}, CFC_{12} and CFC_{13} in anoxic shallow aquifers of Araihazar, Bangladesh. J. Contam. Hydrol. 97 (1), 27–41.
Hudson, N., Baker, A., Reynolds, D., 2007. Fluorescence analysis of dissolved organic matter in natural, waste and polluted waters - a review. River Res. Appl. 23, 631–649.
IAEA/WMO, 2015. Global Network of Isotopes in Precipitation. The GNIP Database. (http://www.iaea.org/water, accessed 15 Feb 2016). .
Islam, F.S., et al., 2004. Role of metal-reducing bacteria in arsenic release from Bengal delta sediments. Nature 430, 68–71.
Javed, M.B., Kachanoski, G., Siddique, T., 2013. A modified sequential extraction method for arsenic fractionation in sediments. Anal. Chim. Acta 787, 102–110.
Jones, K.L., et al., 2014. Atmospheric noble gases as tracers of biogenic gas dynamics in a shallow unconfined aquifer. Geochim. Cosmochim. Acta 128, 144–157.
Khalil, M., Rasmussen, R., 1989. The potential of soils as a sink of chlorofluorocarbons and other man-made chlorocarbons. Geophys. Res. Lett. 16 (7), 679–682.
Klump, S., et al., 2006. Groundwater dynamics and arsenic mobilization in Bangladesh assessed using noble gases and tritium. Environ. Sci. Technol. 40, 243–250.
Kocar, B.D., et al., 2008. Integrated biogeochemical and hydrologic processes driving arsenic release from shallow sediments to groundwaters of the Mekong delta. Appl. Geochem. 23 (11), 3059–3071.
Kocar, B.D., Benner, S.G., Fendorf, S., 2014. Deciphering and predicting spatial and temporal concentrations of arsenic within the Mekong Delta aquifer. Environ. Chem. 11, 579–594.
Kulkarni, H.V., et al., 2017. Contrasting dissolved organic matter quality in groundwater in Holocene and Pleistocene aquifers and implications for influencing arsenic mobility. Appl. Geochem. 77 (194–205).
Lapworth, D.J., Kinniburgh, D.G., 2009. An R script for visualising and analysing fluorescence excitation-emission matrices (EEMs). Comput. Geosci. 35, 2160–2163.
Lapworth, D.J., et al., 2018. Security of deep groundwater in the coastal Bengal Basin revealed by tracers. Geophys. Res. Lett. 45.
Lawrence, A.R., et al., 2000. Groundwater evolution beneath Hat Yai, a rapidly developing city in Thailand. Hydrogeol. J. 8, 564–575.
Lawson, M., et al., 2008. The geochemical and isotopic composition of ground waters in West Bengal: tracing ground-surface water interaction and its role in arsenic release. Mineral. Mag. 72 (1), 441–444.
Lawson, M., et al., 2013. Pond-derived organic carbon driving changes in arsenic hazard found in Asian groundwaters. Environ. Sci. Technol. 47, 7085–7094.
Lawson, M., et al., 2016. Tracing organic matter composition and distribution and its role on arsenic release in shallow Cambodian groundwaters. Geochim. Cosmochim. Acta 178, 160–177.
Lucas, L.L., Unterweger, M.P., 2000. Comprehensive review and critical evaluation of the half-life of tritium. J. Res. Natl. Inst. Stand. Technol. 105 (4), 541.
Magnone, D., et al., 2017. Biomarker-indicated extent of oxidation of plant-derived organic carbon (OC) in relation to geomorphology in an arsenic contaminated Holocene aquifer, Cambodia. Sci. Rep. 7 (13093).
Magnone, D., et al., A new $^{87}Sr/^{86}Sr$ based ^{14}C correction model for dating the oxidised organic carbon contribution to groundwater inorganic carbon. Geochim. Cosmochim. Acta, (under review).
Mai, N.T.H., et al., 2014. Adsorption and desorption of arsenic to aquifer sediment on the Red River floodplain at Nam Du, Vietnam. Geochim. Cosmochim. Acta 142, 587–600.
Mailloux, B.J., et al., 2013. Advection of surface-derived organic carbon fuels microbial reduction in Bangladesh groundwater. PNAS 110 (13), 5331–5335.
Mamyrin, B.A., Tolstikhin, I.N., 1984. Helium Isotopes in Nature. Elsevier, Amsterdam.
Massmann, G., Sültenfuß, J., Pekdeger, A., 2009. Analysis of long-tern dispersion in a river-recharged aquifer using tritium/helium data. Water Resour. Res. 45, W02431.
McArthur, J., et al., 2001. Arsenic in groundwater: testing pollution mechanisms for sedimentary aquifers in Bangladesh. Water Resour. Res. 37 (1), 109–117.
McArthur, J.M., et al., 2004. Natural organic matter in sedimentary basins and its relation to arsenic in anoxic ground water: the example of West Bengal and its worldwide implications. Appl. Geochem. 19 (8), 1255–1293.
McArthur, J.M., et al., 2008. How paleosols influence groundwater flow and arsenic pollution: a model from the Bengal Basin and its worldwide implication. Water Resour. Res. 44.
McArthur, J.M., et al., 2010. Migration of As, and $^{3}H/^{3}He$ ages, in groundwater from West Bengal: implications for monitoring. Water Res. 44 (14), 4171–4185.
McArthur, J.M., Ravenscroft, P., Sracek, O., 2011. Aquifer arsenic source. Nat. Geosci. 4 (10), 655–656.
McKnight, D.M., et al., 1992. Sorption of dissolved organic carbon by hydrous aluminum and iron oxides occurring at the confluence of Deer Creek with the Snake River, Summit County, Colorado. Environ. Sci. Technol. 26 (7), 1388–1396.
Mladenov, N., et al., 2010. Dissolved organic matter sources and consequences for iron and arsenic mobilization in Bangladesh aquifers. Environ. Sci. Technol. 44 (1), 123–128.
Morris, B.L., et al., 2006a. Assessing the impact of modern recharge on a sandstone aquifer beneath a suburb of Doncaster, UK. Hydrogeol. J. 14 (6), 979–997.
Morris, B.L., et al., 2006b. Assessing the extent of induced leakage to an urban aquifer using environmental tracers: an example from Bishkek, capital of Kyrgyzstan, Central Asia. Hydrogeol. J. 14 (1–2), 225–243.
Neumann, R.B., et al., 2009. Hydrology of a groundwater-irrigated rice field in Bangladesh: seasonal and daily mechanisms of infiltration. Water Resour. Res. 45, 14.
Neumann, R.B., et al., 2010. Anthropogenic influences on groundwater arsenic concentrations in Bangladesh. Nat. Geosci. 3 (1), 46–52.
Neumann, R.B., et al., 2011. Aquifer arsenic source reply. Nat. Geosci. 4, 656.
Neumann, R.B., et al., 2014. Biodegradable organic carbon in sediments of an arsenic-contaminated aquifer in Bangladesh. Environ. Sci. Technol. Lett. 1, 221–225.
Nickson, R.T., et al., 1998. Arsenic poisoning of Bangladesh groundwater. Nature 395, 338.
Oster, H., Sonntag, C., Münnich, K., 1996. Groundwater age dating with chlorofluorocarbons. Water Resour. Res. 32 (10), 2989–3001.
Papacostas, N.C., et al., 2008. Geomorphic controls on groundwater arsenic distribution in the Mekong River Delta, Cambodia. Geology 36 (11), 891–894.
Parlanti, E., et al., 2000. Dissolved organic matter fluorescence spectroscopy as a tool to estimate biological activity in a coastal zone submitted to anthropogenic inputs. Org. Geochem. 31, 1765–1781.
Peters, S.C., 2008. Arsenic in groundwaters in the Northern Appalachian Mountain belt: a review of patterns and processes. J. Contam. Hydrol. 99, 8–21.
Plummer, L., Busenberg, E., Cook, P., 2006. Use of Chlorofluorocarbons in Hydrology. International Atomic Energy Agency, Vienna, Austria.
Polizzotto, M.L., et al., 2008. Near-surface wetland sediments as a source of arsenic release to ground water in Asia. Nature 454, 505–508.
Polya, D.A., Charlet, L., 2009. Rising arsenic risk? Nat. Geosci. 2 (6), 383–384.
Polya, D.A., Watts, M.J., 2017. Chapter 5: sampling and analysis for monitoring arsenic in drinking water. In: Bhattacharya, P., Polya, D.A., Jovanovic, D. (Eds.), Best Practice Guide on the Control of Arsenic in Drinking Water. IWA Publishing. ISBN: 9781843393856.
Polya, D.A., et al., 2003. Coupled HPLC-ICP-MS analysis indicates highly hazardous concentrations of dissolved arsenic species in Cambodian groundwaters. R. Soc. Chem. Spec. Publ. 288, 127–140.
Polya, D.A., et al., 2005. Arsenic hazard in shallow Cambodian groundwaters. Mineral. Mag. 69 (5), 807–823.
Polya, D.A., et al., 2017. Chapter A14: Groundwater sampling, arsenic analysis and risk communication: Cambodia Case Study. In: Bhattacharya, P., Polya, D.A., Jovanovic, D. (Eds.), Best Practice Guide for the Control of Arsenic in Drinking Water. IWA Publishing. ISBN: 9781843393856.
Postma, D., et al., 2007. Arsenic in groundwater of the Red River floodplain, Vietnam: controlling geochemical processes and reactive transport modeling. Geochim. Cosmochim. Acta 71 (21), 5054–5071.
Postma, D., et al., 2012. Groundwater arsenic concentrations in Vietnam controlled by sediment age. Nat. Geosci. 5, 656–661.
Postma, D., et al., 2016. A model for the evolution in water chemistry of an arsenic contaminated aquifer over the last 6000 years, Red River floodplain, Vietnam. Geochim. Cosmochim. Acta 195, 277–292.
Radloff, K.A., et al., 2007. Mobilization of arsenic during one-year incubations of grey aquifer sands from Araihazar, Bangladesh. Environ. Sci. Technol. 41, 3639–3645.

Radloff, K.A., et al., 2017. Reversible adsorption and flushing of arsenic in a shallow, Holocene aquifer of Bangladesh. Appl. Geochem. 77, 142–157.
Ravenscroft, P., Brammer, H., Richards, K., 2009. Arsenic pollution - a global synthesis. Royal Geographical Society With IBG. Wiley-Blackwell, Chichester, p. 588.
Richards, L.A., et al., 2015. Use of lithium tracers to quantify drilling fluid contamination for groundwater monitoring in Southeast Asia. Appl. Geochem. 63, 190–202.
Richards, L.A., et al., 2017a. High resolution profile of inorganic aqueous geochemistry and key redox zones in an arsenic bearing aquifer in Cambodia. Sci. Total Environ. 590–591, 540–553.
Richards, L.A., et al., 2017b. Tritium tracers of rapid surface water ingression into arsenic-bearing aquifers in the lower Mekong Basin, Cambodia. Procedia Earth Planet. Sci. 17C, 849–852.
Richards, L.A., et al., 2018. Delineating sources of groundwater recharge in an arsenic-affected Holocene aquifer in Cambodia using stable isotope-based mixing models. J. Hydrol. 557, 321–334.
Richards, L.A., et al., Dissolved organic matter tracers reveal contrasting characteristics across an arsenic bearing aquifer in Cambodia: a fluorescence spectroscopy study. submitted to Geoscience Frontiers, (under review)
Richards, L.A., et al., Contrasting sorption behaviours affected groundwater arsenic concentraiton in Kandal Province, Cambodia. Geosci. Front., (under review).
von Rohden, C., et al., 2010. Accumulation of natural SF_6 in the sedimentary aquifers of the North China Plain as a restriction on groundwater dating. Isot. Environ. Health Stud. 46 (3), 279–290.
Rowland, H.A.L., et al., 2007. The control of organic matter on microbially mediated iron reduction and arsenic release in shallow alluvial aquifers, Cambodia. Geobiology 5, 281–292.
Rowland, H.A.L., et al., 2008. Geochemistry of aquifer sediments and arsenic-rich groundwaters from Kandal Province, Cambodia. Appl. Geochem. 23 (11), 3029–3046.
Rowland, H.A.L., et al., 2009. The role of indigenous mircoorganisms in the biodegradation of naturally occurring petroleum, the reduction of iron, and the mobilization of arsenite from West Bengal aquifer sediments. J. Environ. Qual. 38 (4), 1598–1607.
Santella, N., et al., 2008. Widespread elevated atmospheric SF_6 mixing ratios in the northeastern United States: implications for groundwater dating. J. Hydrol. 349 (1), 139–146.
Schaefer, M.V., et al., 2016. Aquifer arsenic cycling induced by seasonal hydrologic changes within the Yangtze River Basin. Environ. Sci. Technol. 50 (7), 3521–3529.
Schlosser, P., et al., 1989. Tritiogenic ^{3}He in shallow groundwater. Earth Planet. Sci. Lett. 94, 245–256.
Sengupta, S., et al., 2008. Do ponds cause arsenic-pollution of groundwater in the Bengal Basin? An answer from West Bengal. Environ. Sci. Technol. 42, 5156–5164.
Slota, P.J., et al., 1987. Preparation of small samples for ^{14}C accelerator targets by catalytic reduction of CO. Radiocarbon 29, 303–306.
Smedley, P.L., Kinniburgh, D.G., 2002. A review of the source, behaviour and distribution of arsenic in natural waters. Appl. Geochem. 17 (5), 517–568.
Solomon, D.K., Cook, P.G., 2000. ^{3}H and ^{3}He. In: Cook, P.G., Herczeg, A.L. (Eds.), Environmental Tracers in Subsurface Hydrology, pp. 397–424.
Stedmon, C.A., Bro, R., 2008. Characterizing dissolved organic matter fluorescence with parallel factor analysis: a tutorial. Limnol. Oceanogr. Methods 6 (572–579).
Stedmon, C.A., Markager, S., Bro, R., 2003. Tracing dissolved organic matter in aquatic environments using a new approach to fluorescence spectroscopy. Mar. Chem. 82, 239–254.
Stuckey, J.W., et al., 2016. Arsenic release metabolically limited to permanently water-saturated soil in Mekong Delta. Nat. Geosci. 9, 70–76.
Stute, M., et al., 1997. Tritium/^{3}He dating of river infiltration: an example from the Danube in the Szigetköz Area, Hungary. Groundwater 35 (5), 905–911.
Stute, M., et al., 2007. Hydrological control of As concentrations in Bangladesh groundwater. Water Resour. Res. 43, W09417.
Sültenfuß, J., Roether, W., Rhein, M., 2009a. The Bremen mass spectrometric facility for the measurement of helium isotopes, neon, and tritium in water. Isot. Environ. Health Stud. 45 (2), 83–95.
Sültenfuß, J., Osenbrück, K., Weise, S.M., 2009b. Uncertainty assessment of tritiogenic ^{3}He and tritium/^{3}He-ages. Presented at Goldschmidt (Switzerland).
Sültenfuß, J., Purtschert, R., Führböter, J.F., 2011. Age structure and recharge conditions of a coastal aquifer (northern Germany) investigated with ^{39}Ar, ^{14}C, ^{3}H, He isotopes and Ne. Hydrogeol. J. 19, 221–236.
Szabo, Z., et al., 1996. Age dating of shallow groundwater with chlorofluorocarbons, tritium/helium 3, and flow path analysis, southern New Jersey coastal plain. Water Resour. Res. 32 (4), 1023–1038.
Tamura, T., et al., 2007. Depositional facies and radiocarbon ages of a drill core from the Mekong River lowland near Phnom Penh, Cambodia: evidence for tidal sedimentation at the time of Holocene maximum flooding. J. Asian Earth Sci. 29 (5–6), 585–592.
Thoeun, H.C., 2015. Observed and projected changes in temperature and rainfall in Cambodia. Weather Clim. Extremes 7, 61–71.
Thurman, E., 1985. In: M.N.D. W (Ed.), Organic Geochemistry of Natural Waters. Developments in Biogeochemistry. Junk Publishers, Boston, MA.
Tolstikhin, I.N., Kamenskiy, I.L., 1969. Determination of ground-water ages by the T-^{3}He method. Geochem. Int. 6, 810–811.
Uhlemann, S., et al., 2017. Electrical resistivity tomography determines the spatial distribution of clay layer thickness and aquifer vulnerability, Kandal Province, Cambodia. J. Asian Earth Sci. 147, 402–414.
United States Geological Survey (USGS), 2017. The Reston Groundwater Dating Laboratory, Tracer Input Functions. (https://water.usgs.gov/lab/software/air_curve/, accessed February 2018). .
Watts, M.J., et al., 2010. Field based speciation of arsenic in UK and Argentinean water samples. Environ. Geochem. Health 32, 479–490.
Weise, S.M., Moser, H., 1987. Groundwater dating with helium isotopes. Isotope Techniques in Water Resources Development. International Atomic Energy Agency, Vienna, pp. 105–126.
Weiss, R.F., 1971. Solubility of helium and Neon in water and seawater. J. Chem. Eng. Data 16 (2), 235–241.
Wilson, H.F., Xenopoulos, M.A., 2009. Effects of agricultural land use on the composition of fluvial dissolved organic matter. Nat. Geosci. 2, 37–41.
World Health Organization (Ed.), 2011. Guidelines for Drinking-water Quality, Fourth edition World Health Organization, Geneva.
Xu, S., et al., 2004. Capabilities of the new SUERC 5MV AMS facility for ^{14}C dating. Radiocarbon 46 (1), 59–64.
Yang, Q., et al., 2015. Flow and sorption controls of groundwater arsenic in individual boreholes from bedrock aquifers in central Maine, USA. Sci. Total Environ. 505, 1291–1307.